Polymer Degradation and Stability 94 (2009) 1349–1353

Contents lists available at ScienceDirect

Polymer Degradation and Stability

journal homepage: www.elsevier.com/locate/polydegstab

Self-assemblies of enzymatically degradable amphiphilic oligopeptides as nonviral gene carrier

Tomoko Hashimoto [a,b], Reiko Iwase [b,c], Akira Murakami [b], Tetsuji Yamaoka [a,b,*]

[a] Department of Biomedical Engineering, National Cardiovascular Center Research Institute, 5-7-1 Fujishirodai, Suita, Osaka 565-8565, Japan
[b] Department of Biomolecular Engineering, Kyoto Institute of Technology, Matsugasaki, Sakyo-ku, Kyoto 606-8585, Japan
[c] Department of Biosciences, Teikyo University of Science and Technology, 2525 Yatsusawa, Uenohara, Yamanashi 409-0193, Japan

ARTICLE INFO

Article history:
Received 25 April 2009
Received in revised form
25 May 2009
Accepted 28 May 2009
Available online 6 June 2009

Keywords:
Polymeric gene carrier
Self-assembly
Stability
Oligopeptide
Molecular weight

ABSTRACT

Novel biodegradable oligopeptide-type gene carriers composed of cationic residues (KRRRKRKRRRKRKRRC) and oligo leucine segments were developed. The amphiphilic carrier was found to form micelle-like assemblies in aqueous solutions, when the oligo leucine is 12 amino acids length (Pep-L12). NMR, CMC, and GPC analysis revealed their hydrophobic/cationic core/shell morphology. Hydrophobic interaction between leucines is thought to be the major driving force behind formations of assemblies. The transient expression of luciferase introduced to COS-1 cells using Pep-L12 below the CMC is as low as that by the control cationic peptides without leucine residue (Pep-L0), while improved transgene expression was observed in the case of Pep-L12 above CMC. The self-assembly raised the apparent molecular weight and gene transfection ability without loosening their low cytotoxicity. These results indicate that the amphiphilic oligopeptides are very promising materials as highly efficient and less toxic gene carriers.

1. Introduction

Polymeric gene carriers are now extensively studied due to their high abilities to deliver and protect pDNA, but the polyplexes formed between the carriers and pDNAs are sometimes too highly compacted to be recognized by transcription factors in nucleus. Recently, the destabilization of the polyplexes by conjugating hydrophilic or hydrophobic segments to polymeric carriers has been reported [1–3]. However, excess modification of side chains results in the low resistance to DNase at the same time.

Effect of the carrier molecular weights (Mws) has been also being studied [4–8]. Recently, high potential of low Mw polymeric carriers was attracting great attention. Kunath et al. reported that low Mw PEI (5 kDa) was much less toxic than high Mw PEI (48 kDa), and reporter gene expression of 5 kDa PEI was 3.7-fold higher than 48 kDa PEI in various cell lines [6]. Breuning et al. compared PEIs with the Mw of 1–9 kDa and showed that the highest reporter gene expression was obtained at 5.6 kDa, with low cytotoxicity. Schaffer et al. reported higher gene expression for low Mw PLL (19 and 36 residues) than high Mw PLL (180 residues) because of effective *in vitro* transcription and easy pDNA release [4]. Taken together, low cytotoxicity and high DNA releasing ability of low Mw carries were important key features for the high potential gene carriers. On the other hand, low Mw carriers are pointed out to reduce cellular uptake [9] and decrease stability of polyplexes at the same time. Thus, a new type "low Mw carriers", which have low cytotoxicity, high cellular uptake, and adequate polyplex stability, would be more useful gene carriers.

In the present study, oligopeptide-type carriers were selected in order to reduce cytotoxicity and to induce the intracellularly digestible feature. Since the chemical chain elongation of cationic oligopeptide would increase the cytotoxicity, we tried to raise the apparent Mw of oligopeptide-type carriers by their self-assembly. Amphiphilic oligopeptides having cationic and hydrophobic sequences were then designed. Hydrophobic interactions between oligo leucine sequences make carriers form assemblies and increase the apparent Mw. Cationic sequences for interacting with pDNA include cleavable sequences (Arg-X-Lys/Arg-Arg (R-X-K/R-R)) by intracellular proprotein convertase, furin [10,11]. We have previously found that carriers including this cleavable sequences are enough cationic to form polyplexes with pDNA, and these polyplexes became destabilized if carriers were cleaved by furin [12]. Increased apparent Mw is expected to increase cellular uptake of the polyplex and the enhanced stability can be destabilized by furin cleavage resulting in the pDNA release in intracellular environments.

* Corresponding author at: Department of Biomedical Engineering, National Cardiovascular Center Research Institute, 5-7-1 Fujishirodai, Suita, Osaka 565-8565, Japan. Tel.: +81 6 6833 5012x2637; fax: +81 6 6835 5476.
E-mail address: yamtet@ri.ncvc.go.jp (T. Yamaoka).

0141-3910/$ – see front matter © 2009 Elsevier Ltd. All rights reserved.
doi:10.1016/j.polymdegradstab.2009.05.021

2. Experimental

2.1. Amphiphilic oligopeptides

We synthesized four oligopeptides by Fmoc-based solid phase method using 9050 plus PepSynthesizer (Applied Biosystems, CA, USA) and purified in the usual way. They are composed of cationic KRRRKRKRRRKRKRRC and hydrophobic oligo leucine segment with different lengths.

Oligopeptide solutions were analyzed by GPC (Shimadzu Corporation, Kyoto, Japan) which fitted with a combination of two columns of TSK gel G6000PWXL (21.5 mm I.D. × 300 mm length, Tosoh Corporation, Tokyo, Japan) and TSK gel G3000PWXL, RID-10A Refractive index detector, and SPD-M10A UV–VIS detector. Elution was carried out with 1/15 M phosphate buffer (pH 7.5) at 0.3 mL/min.

2.2. Critical micelle concentration (CMC) measurements

CMCs of oligopeptides in aqueous solution were measured on a RF5300PC (Shimadzu Corporation, Kyoto, Japan) using pyrene (Nacalai Tesque, Inc., Kyoto, Japan) as a hydrophobic region probe [13]. Five μL of pyrene solution in acetone at a concentration of 6×10^{-5} M was transferred into a vial and evaporated. Five hundred μL of oligopeptide solutions which ranging from 5.0×10^{-4}–1.5 g/L were added dropwise to make the pyrene concentration of 6.0×10^{-7} M, incubated at 65 °C for 3 h, and cooled down to the room temperature. Pyrene excitation spectra were measured with the slit widths of 5 and 1.5 nm for excitation and emission at an emission wavelength of 380 nm.

2.3. Polyplex formation with pDNA

pCMV-Luc and pT7-Luc (Promega corporation, WI, USA) were amplified to sufficient quantities by standard molecular biology techniques, and purified with a QIAGEN-tip 500 (QIAGEN K.K., Tokyo, Japan). Oligopeptide solutions were mixed with pDNA solutions at a given charge ratio which is the ratio of the number of cationic groups of oligopeptide to that of anionic group of pDNA (*C/A* ratio). The solutions were incubated for 30 min at 37 °C to allow the polyplex formation and analyzed on 0.8 wt% agarose gel in Tris–borate EDTA buffer at 100V for 30 min. pDNA was visualized by staining with 0.5 μg/mL ethidium bromide (EtBr, Sigma chemicals, St Louis, MO, USA).

2.4. In vitro *transfection*

COS-1 cells were grown in DMEM (Nissui, Tokyo, Japan) containing 10% fetal bovine serum (FBS) (Sigma chemicals, USA) at 37 °C under a 5% CO_2 atmosphere. COS-1 cells were seeded in 96 well culture plates at a density of 1×10^4 in 100 μL DMEM containing 10% FBS per well. After 24 h incubation, cells were washed with PBS, and 40 μL DMEM was added. Ten μL of polyplex solutions containing 100 ng pCMV-Luc at the concentration above or below CMC of Pep-L12 were poured gently to the wells. Fifty μL of 200 μM chloroquine solution was added (final concentration is 100 μM) and incubated for 5 h. Cells were washed with PBS and cultured for 43 h with DMEM containing 10% FBS at 37 °C in a 5% humidified CO_2 environment. The cells were washed with PBS, treated with the lysis buffer containing 1% Triton-X100, and incubated for 30 min at 37 °C. Cell lysate was diluted into luciferase assay solution containing 470 μM luciferin. The relative light units (RLU) of expressed luciferase were measured using ATP-300 Lumicounter (Advantec Toyo Kaisya, Ltd., Tokyo, Japan). Luciferase solutions at a known concentration were used for calibration. The protein concentration was determined by DC Protein Assay kit (Bio-Rad Laboratories, Hercules, CA, USA) using bovine serum albumin as a standard. The obtained luciferase expression (ng luciferase) was divided by total protein content of cell lysates and expressed as ng luciferase/mg protein.

Table 1
Sequences of amphiphilic oligopeptides.

Oligopeptide	Sequences and cleavage sites	Amino acid composition (K/R/L/C)
Pep-L0	H_2N-K-R-R-R-K-R*-K-R-R*-R-K-R*-K-R-R*-C-$CONH_2$	10/5/0/1
Pep-L4	H_2N-$(L)_4$-K-R-R-R-K-R*-K-R-R*-R-K-R*-K-R-R*-C-$CONH_2$	10/5/4/1
Pep-L8	H_2N-$(L)_8$-K-R-R-R-K-R*-K-R-R*-R-K-R*-K-R-R*-C-$CONH_2$	10/5/8/1
Pep-L12	H_2N-$(L)_{12}$-K-R-R-R-K-R*-K-R-R*-R-K-R*-K-R-R*-C-$CONH_2$	10/5/12/1

* represents the cleavage site of furin.

2.5. Cell-free assay system for luciferase expression

Fifteen μL of polyplexes ($C/A = 10$) were mixed with 12.8 μL of rabbit reticulocyte lysate mixtures (T_NT Coupled Reticulocyte Lysate Systems; Promega, WI, USA) and incubated with shake at rate of 300 rpm/min for 90 min at 30 °C. After transcription/translation assay according to the manufacture's protocol, luciferase activities were measured by the same method described in the above section.

3. Results and discussion

3.1. Self-assembly of amphiphilic carriers

Sequences and abbreviation of synthesized amphiphilic oligopeptides were shown in Table 1. GPC chart for each amphiphilic oligopeptide in phosphate buffer is shown in Fig. 1. Only Pep-L12 exhibited two peaks, while the other oligopeptides showed peak which is at the similar elution time to the second peak of Pep-L12. The first peak of Pep-L12 is considered to be attributed to the self-assembly of the Pep-L12 with the apparent higher Mw and the second peak corresponds to the unimer as low Mw as the other oligopeptides, Pep-L0, Pep-L4, and Pep-L8. These results indicated that only Pep-L12 forms micelle-like assemblies in aqueous solution.

Micelle-like assemblies can be confirmed by comparing ^1H NMR spectra in good solvents and water [14,15]. Protons in the core structure composed of the insoluble fractions do not provide sufficient NMR signals. Thus, self-assembly of oligopeptides was analyzed in DMSO and water. Leucine contents (X_{Leu}) in water and in DMSO were measured using the signal intensity at 0.8 ppm (CH_3 in leucine) and at 1.6 ppm (β-CH_2 and γ-CH in leucine, β, γ, and δ-CH_2 in lysine, β and γ-CH_2 in arginine, and SH in cysteine). The

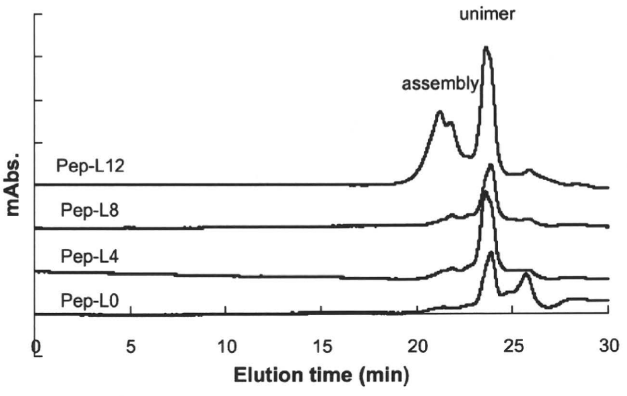

Fig. 1. GPC charts of Pep-LX (X = 0, 4, 8 and 12).

relative value of [X_{Leu} in water]/[X_{Leu} in DMSO] for Pep-L4 and Pep-L8 were 1.00 and 1.08, respectively, indicating that these oligopeptides has a same structure in both of medium. On the other hand, [X_{Leu} in water]/[X_{Leu} in DMSO] for Pep-L12 was 0.69, which strongly supports the oligo leucine/oligo cation core/shell structure of Pep-L12 in water.

3.2. CMC measurements

The excitation spectra of pyrene in oligopeptides solutions at various concentrations were measured. Fig. 2 demonstrates the intensity ratios ($I_{338.6}/I_{330.4}$) as a function of the logarithm of Pep-L12 concentration. As Pep-L12 concentration increased, the intensity ratio start increasing at a certain concentration, suggesting that pyrene molecules were incorporated into hydrophobic region upon assembly formation. CMC of Pep-L12 is determined from the crossover point was 0.16 g/L. This CMC is very high compared with reported CMC of other amphiphilic polymers [13,16]. This result suggested that Pep-L12 forms unstable assemblies resulting from weak hydrophobic interaction between leucine residues. In case of Pep-L8, a crossover point was not obtained. Hydrophobic interactions of Pep-L8 seem to be not strong enough to form assemblies in aqueous solution, which is in agreed with the GPC chart in Fig. 1. In addition, Pep-L12 assemblies were observed in AFM images above CMC (data not shown). While there were no assemblies at the lower concentration than CMC.

3.3. Polyplex formation

Fig. 3 shows the polyplex formation of the Pep-L12 at various *C/A* ratios. When Pep-L12 was mixed with pDNA, bands for free pDNA disappeared at the *C/A* ratio of 5, indicating that all pDNA form polyplexes with carriers. Concentrations of polyplex formation above and below CMC were same, indicating the polyplex forming ability of the micelle-like self-assembly of the Pep-L12 is same to that for Pep-L12 unimer. This phenomenon can be elucidated by the micelle-like architecture, which cationic residues are covering the hydrophobic core. The net amount of the cationic groups was then not significantly changed upon the self-assembly. Pep-L0 also formed polyplexes completely from *C/A* ratio of 5 similar to Pep-L12 (data not shown).

3.4. In vitro gene transfection

COS-1 cells were transfected with pCMV-Luc using Pep-L12 and Pep-L0 at various *C/A* ratio, and the transient expressions of

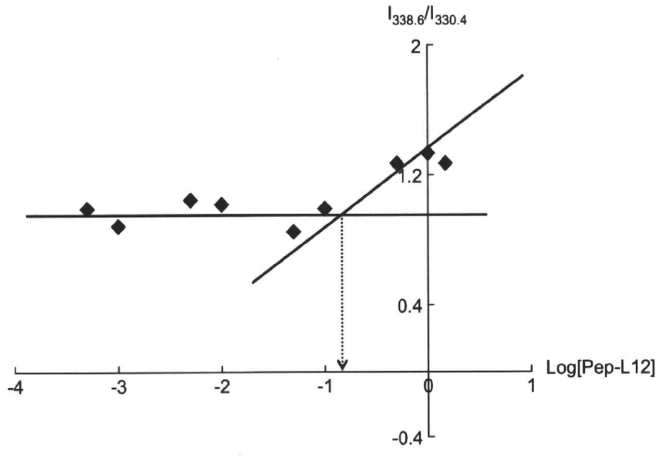

Fig. 2. $I_{338.6}/I_{330.4}$ in pyrene excitation spectra versus Pep-L12 concentration. CMC of Pep-L12 was 0.16 g/L.

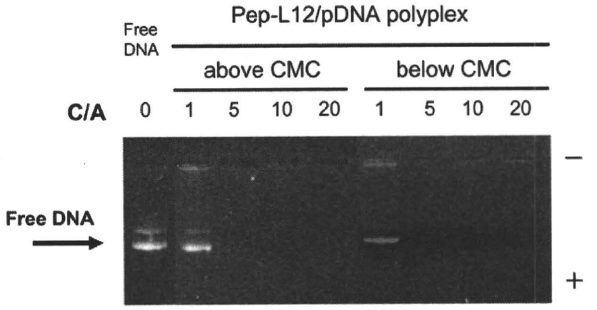

Fig. 3. Comparison of electrophoretic mobility profiles of Pep-L12 polyplexes. Polyplexes were analyzed at various *C/A* ratios on an agarose gel (0.8 wt%). Left five lanes represent polyplexes containing 200 ng pDNA above CMC and right four lanes are those containing 100 ng pDNA below CMC.

luciferase gene were evaluated. Cell viabilities for Pep-L12 and Pep-L0 by after transfection procedure were higher than 80% (data not shown). In general, high Mw polycations have profound cell damages, but the cytotoxicity of Pep-L12 above CMC is low. As is shown in Fig. 4(b), both Pep-L0 and Pep-L12 oligopeptides did not work as gene carriers in the unimer forms. However, only Pep-L12 did lead to improved transgene expression as increasing *C/A* ratio when used as the micelle-like architecture above the CMC (Fig. 4(a)). Luciferase expression for Pep-L12 and Pep-L0 was 220.0 ± 68.0 and 19.3 ± 0.2 ng luciferase/mg protein at *C/A* ratio of 10, respectively. Under the same condition, we confirmed that the luciferase expression for oligoarginine (16 mer) was 2.4 ± 0.7 ng luciferase/mg protein at *C/A* ratio of 8 (data not shown). Luciferase expression for Pep-L12 was 100-fold higher than that for widely studied oligoarginine [17], indicating that Pep-L12 is a useful gene carrier.

Possible reasons for improved transfection efficiency by Pep-L12 micell-like carrier is discussed below. First, pDNA uptake was improved because of the high apparent Mw. It was reported that cellular uptakes were increased as increasing in carrier Mw [9,18]. The second reason is the resistance of pDNA to DNase. We have studied the DNase I resistance of polyplexes for poly-L-lysine (from 15 to 1170 mer) or poly-L-arginine (from 70 to 650 mer) by incubating polyplexes with DNase I *in vitro*. As results, higher Mw polypeptide leads to the larger DNase resistance may be because of the large compaction of the polyplexes (data not shown).

Enhanced transcription is the third possible reason for the improved luciferase expression. We previously reported that a micelle-type polycation is superior to the linear-type polycation in gene transfer due to the enhanced transcription [2]. In addition, we found the enhanced gene expression of the linear-type oligopeptide composed of furin cleavage sequences in comparison to control sequences without cleavage sites [12]. These results indicated that the intracellular cleavage of the cationic residues in Pep-L12 self-assembly by intracellular furin enzyme might play a role in weakening the polyplex compaction by decreasing the charge density of the cationic micelle-like architecture.

3.5. Transcription/translation efficiency in cell-free system

To elucidate the reason for enhanced transgene expression, cell-free transcription/translation assay was performed using Pep-L0 and Pep-L12. The transcription efficiency of Pep-L12 was suppressed completely in comparison with free pT7-Luc, but Pep-L0 showed slightly residual transcription (Fig. 5). In general, polyplexes composed of high Mw polycation are strongly compacted and then hard to be transcribed. As is similarly, Pep-L12 forming micelle-like structure seems to suppress transcription in cell-free system. However, Pep-L12 successfully led to the transgene

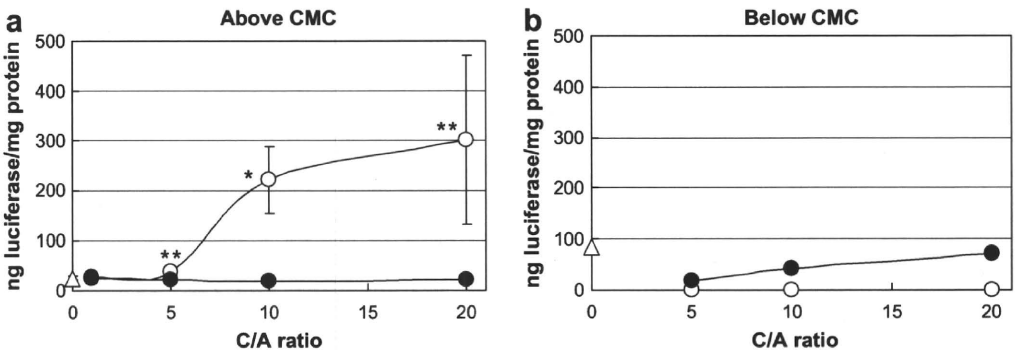

Fig. 4. Transient luciferase expression in COS-1 cells transfected using Pep-L0 (●) and Pep-L12 (○) in the presence of 100 μM chloroquine. (△) represents results for naked pCMV-Luc. Transfection assays were perfumed at above (a) or below (b) CMC of Pep-L12. (*$P < 0.01$, **$P < 0.05$.)

expression above CMC when evaluated in COS-1 system (Fig. 4), which indicates that the intracellular furin is able to associate with Pep-L12 somehow in cells.

In the present study, hydrophobic modification of the cationic gene carriers was proved to be effective. Pep-L12 formed hydrophobic/cationic core/shell morphology in aqueous solutions and lead to the enhanced gene expression *in vitro*. This type of core-shell structure should be energetically stable but the inverse structure has been also proposed. Futaki et al. reported that stearylated octaarginine forms polyplexes with the hydrophobic stearyl moieties at the outer surface and induces enhanced transgene expressions due to earlier endosomal escape. They expected that hydrophobic moieties contributed to interactions between polyplexes and cell membranes [19]. In our system, the leucine residues form core structure covered by the charged group and then it worked in the different mechanism.

In order to improve gene delivery efficiency with minimum cytotoxicity, several groups have reported the cross-linking of small PEIs with biodegradable linkage. Linked PEIs presented effective transgene expressions close to or higher than that offered by high Mw PEI (25 kDa) with reduced cytotoxicity [20,21]. Although low Mw PEI is much less cytotoxic than high Mw PEI, undegradable PEI remaining inside cells for a long period of time might interact with cell organelles and affect on cell functions [21]. On the other hand, oligopeptides would be understandably degraded if they remain inside cells after transfection. In this work, we designed novel oligopeptide-type carriers which showed high apparent Mw in aqueous solutions. Synthetic nonviral gene carriers composed of oligopeptides are thought to have potential of low cytotoxicity, enhanced cellular uptake and resistance to DNase. Further researches are necessary to clarify the intracellular behavior, physicochemical properties of polyplexes, such as degree of compaction and surface charge density.

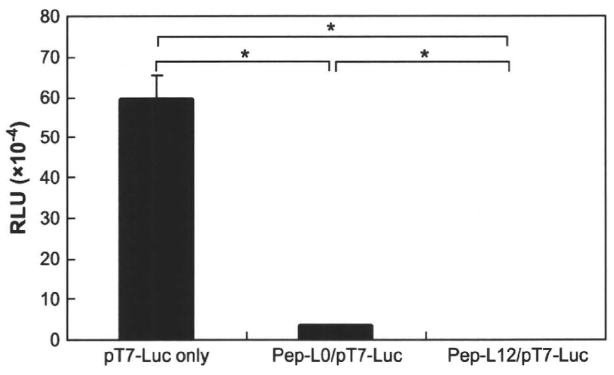

Fig. 5. Transcription efficiency determined by luciferase activity in *in vitro* transcription/translation system at *C/A* of 10. Polyplex formation was perfumed at a higher concentration than CMC of Pep-L12. (*$P < 0.0001$.)

4. Conclusions

A novel amphiphilic carrier Pep-L12 was synthesized by conjugating cationic sequences and hydrophobic sequences. Pep-L12 formed assemblies in aqueous solution at concentration above 0.16 g/L. Formations of assemblies brought about a dramatic increasing apparent Mw of carriers. Assemblies led enhanced transgene expression than linear carriers. Further analysis has to be done to design more effective self-assembly type gene carrier with low cytotoxicity.

Acknowledgements

We thank to Prof. Osam Mazda of Kyoto Prefectural University of Medicine for his great suggestion. This work was partly supported by Grants for Regional Science and Technology Promotion from the Ministry of Education, Culture, Sports, Science and Technology.

References

[1] Kimura T, Yamaoka T, Iwase R, Murakami A. Effect of physicochemical properties of polyplexes composed of chemically modified PL derivatives on transfection efficiency in vitro. Macromol Biosci 2002;2:437–46.
[2] Kitagawa T, Iwase R, Ishihara K, Yamaoka T, Murakami A. Facilitated disassembly of polyplexes composed of self-assembling amphiphilic polycations enhances the gene transfer efficacy. Chem Lett 2005;34(11):1478–9.
[3] Honore I, Grosse S, Frison N, Favatier F, Monsigny M, Fajac I. Transcription of plasmid DNA: influence of plasmid DNA/polyethylenimine complex formation. J Control Release 2005;107(3):537–46.
[4] Schaffer DV, Fidelman NA, Dan N, Lauffenburger DA. Vector unpacking as a potential barrier for receptor-mediated polyplex gene delivery. Biotechnol Bioeng 2000;67(5):598–606.
[5] Godbey WT, Wu KK, Mikos AG. Size matters: molecular weight affects the efficiency of poly(ethylenimine) as a gene delivery vehicle. J Biomed Mater Res 1999;45(3):268–75.
[6] Kunath K, VH A, Fischer D, Petersen H, Bickel U, Voigt K, et al. Low-molecular-weight polyethylenimine as a non-viral vector for DNA delivery: comparison of physicochemical properties, transfection efficiency and in vivo distribution with high-molecular-weight polyethylenimine. J Control Release 2003;89(1):113–25.
[7] Breunig M, Lungwitz U, Liebl R, Fontanari C, Klar J, Kurtz A, et al. Gene delivery with low molecular weight linear polyethylenimines. J Gene Med 2005;7(10):1287–98.
[8] Bettinger T, Carlisle RC, Read ML, Ogris M, Seymour LW. Peptide-mediated RNA delivery: a novel approach for enhanced transfection of primary and post-mitotic cells. Nucleic Acids Res 2001;29(18):3882–91.
[9] Varga CM, Tedford NC, Thomas M, Klibanov AM, Griffith LG, Lauffenburger DA. Quantitative comparison of polyethylenimine formulations and adenoviral vectors in terms of intracellular gene delivery processes. Gene Ther 2005;12(13):1023–32.
[10] Hosaka MNM, Kim WS, Watanabe T, Hatsuzawa K, Ikemizu J, Murakami K, et al. Arg-X-Lys/Arg-Arg motif as a signal for precursor cleavage catalyzed by furin within the constitutive secretory pathway. J Biol Chem 1991;266(19):12127–30.

[11] Molloy SSBP, Leppla SH, Klimpel KR, Thomas G. Human furin is a calcium-dependent serine endoprotease that recognizes the sequence Arg-X-X-Arg and efficiently cleaves anthrax toxin protective antigen. J Biol Chem 1992;267(23):16396–402.
[12] Hashimoto T, Tachibana Y, Nozaki H, Mazda O, Niidome T, Murakami A, et al. Intracellular enzyme-responsive fragmentation of nonviral gene carriers leads to polyplex destabilization and enhanced transgene expression. Chem Lett, in press.
[13] Lee KY, Kwon IC, Kim YH, Jo WH, Jeong SY. Preparation of chitosan self-aggregates as a gene delivery system. J Control Release 1998;51(2–3):213–20.
[14] Liu M, Kono K, Frechet JMJ. Water-soluble dendritic unimolecular micelle: their potential as drug delivery agents. J Control Release 2000;65(1–2):121–31.
[15] Jette KK, Law D, Schmitt EA, Kwon GS. Preparation and drug loading of poly(ethylene glycol)-block-poly(ε-caprolactone) micelles through the evaporation of a cosolvent azeotrope. Pharm Res 2004;21(7):1184–91.
[16] Zhang J, Wang LQ, Wang H, Tu K. Micellization phenomena of amphiphilic block copolymers based on methoxy poly(ethylene glycol) and either crystalline or amorphous poly(caprolactone-b-lactide). Biomacromolecules 2006;7(9):2492–500.
[17] Fuchs SM, Raines RT. Pathway for polyarginine entry into mammalian cells. Biochemistry 2004;43(9):2438–44.
[18] Wender PA, Mitchell DJ, Pattabiraman K, Pelkey ET, Steinman L, Rothbard JB. The design, synthesis, and evaluation of molecules that enable or enhance cellular uptake: peptoid molecular transporters. Proc Natl Acad Sci U S A 2000;97(24):13003–8.
[19] Futaki S, Ohashi W, Suzuki T, Niwa M, Tanaka S, Ueda K, et al. Stearylated arginine-rich peptides: a new class of transfection systems. Bioconjug Chem 2001;12(6):1005–11.
[20] Thomas M, Ge Q, Lu JJ, Chen J, Klibanov AM. Cross-linked small polyethylenimines: while still nontoxic, deliver DNA efficiently to mammalian cells in vitro and in vivo. Pharm Res 2005;22(3):373–80.
[21] Tang GP, Guo HY, Alexis F, Wang X, Zeng S, Lim TM, et al. Low molecular weight polyethylenimines linked by beta-cyclodextrin for gene transfer into the nervous system. J Gene Med 2006;8(6):736–44.

Available online at www.sciencedirect.com
ScienceDirect
Biomaterials 29 (2008) 1307–1317
Biomaterials
www.elsevier.com/locate/biomaterials

Scaffolds from electrospun polyhydroxyalkanoate copolymers: Fabrication, characterization, bioabsorption and tissue response

Tang H. Ying [a,b], Daisuke Ishii [c], Atsushi Mahara [d], Sunao Murakami [d], Tetsuji Yamaoka [d], Kumar Sudesh [a,b], Razip Samian [b], Masahiro Fujita [a,*], Mizuo Maeda [a], Tadahisa Iwata [c,**]

[a] *Bioengineering Laboratory, RIKEN Institute, 2-1 Hirosawa, Wako-shi, Saitama 351-0198, Japan*
[b] *School of Biological Science, Universiti Sains Malaysia, 11800 Penang, Malaysia*
[c] *Department of Biomaterial Sciences, Graduate School of Agricultural and Life Sciences, The University of Tokyo, 1-1-1 Yayoi, Bunkyo-ku, Tokyo 113-8657, Japan*
[d] *Department of Biomedical Engineering, Advanced Medical Engineering Center, National Cardiovascular Center Research Institute, 5-7-1 Fujishirodai, Suita, Osaka 565-8565, Japan*

Received 10 September 2007; accepted 24 November 2007
Available online 21 December 2007

Abstract

Polyhydroxyalkanoate (PHA) copolymers of poly[(*R*)-3-hydroxybutyrate-*co*-5mol%-(*R*)-3-hydroxyhexanoate], poly[(*R*)-3-hydroxybutyrate-*co*-7mol%-4-hydroxybutyrate] and poly[(*R*)-3-hydroxybutyrate-*co*-97mol%-4-hydroxybutyrate] were electrospun to fabricate scaffolds with enhanced biocompatibility and bioabsorption. Subcutaneous implantation of the fibers in rats was performed to investigate their bioabsorption behavior and tissue response. The fibers before and after the *in vivo* experiments were characterized using gel permeation chromatography, scanning electron microscopy, X-ray diffraction and tensile test. Histological evaluation was also performed to determine the tissue response. The structures and properties of the electrospun PHA copolymers were compared with those of the electrospun poly[(*R*)-3-hydroxybutyrate]. The content and type of the second monomer and the diameter of fiber significantly influence the bioabsorption. The tissue response was found to improve with the high content of 4-hydroxybutyrate.

Keywords: Electrospun fiber; Polyhydroxyalkanoate; Tissue response; Bioabsorption

1. Introduction

In response to the growing demand in the field of tissue engineering, the number of polyhydroxyalkanoates (PHAs) currently under evaluation as biomaterial has expanded to five, that is, poly[(*R*)-3-hydroxybutyrate] [P(3HB)], poly(4-hydroxybutyrate) [P(4HB)], poly[(*R*)-3-hydroxybutyrate-*co*-4-hydroxybutyrate] [P(3HB-*co*-4HB)], poly[(*R*)-3-hydroxybutyrate-*co*-(*R*)-3-hydroxyvalerate] [P(3HB-*co*-3HV)] and poly[(*R*)-3-hydroxyoctanoate-*co*-(*R*)-3-hydroxyhexanoate] [P(3HO-*co*-3HHx)] [1]. To date, PHA and its composites are thought to have good potentials as emerging materials for medical devices such as sutures, bone plates, surgical mesh and cardiovascular patches, just to name a few [2]. A recent major breakthrough for PHA as a new class of biomaterial is the clearance obtained from the Food and Drug Administration of the United States of America for the use of P(4HB)-derived TephaFLEX® absorbable suture [3].

PHAs are a family of biopolyesters produced by numerous bacteria as intracellular carbon and energy compound under unfavorable growth conditions such as limitation of nitrogen, phosphorus, oxygen or magnesium in the presence of excess supply of carbon source [4–6]. PHAs are particularly attractive because they are bioabsorbable and biocompatible. The metabolism and excretion of some monomers incorporated into PHA

* Corresponding author. Tel.: +81 48 467 9312; fax: +81 48 462 4658.
** Corresponding author. Tel.: +81 3 5841 7888; fax: +81 3 5841 1304.
E-mail addresses: mfujita@riken.jp (M. Fujita), atiwata@mail.ecc.u-tokyo.ac.jp (T. Iwata).

0142-9612/$ - see front matter © 2007 Elsevier Ltd. All rights reserved.
doi:10.1016/j.biomaterials.2007.11.031

are well understood. For example, the monomeric component of P(3HB), (*R*)-3-hydroxybutanoic acid (3HB), is a ketone body present at concentrations of 3–10 mg per 100 mL blood in healthy adults [1,7]. The monomeric component of P(4HB), 4-hydroxybutanoic acid (4HB), can also be found widely distributed in the brain, kidney, heart, liver, lung and muscle of the mammalian body [8]. Furthermore, the hydroxyl acids released during PHA *in vivo* breakdown are found to be considerably less acidic and less inflammatory than many currently used synthetic absorbable polymers such as poly(lactic acid) (PLA) [9]. P(3HB) has, however, limited application due to its high brittleness, poor processability and slow degradation [10]. Therefore, researches in this field of interest had shown great progress over the past 20 years and it is now possible to design and synthesize various kinds of PHA (reviewed in Ref. [11]) to overcome the inferior properties of P(3HB).

New polymer processing approaches are in demand to create degradable porous scaffolds that can support the hierarchical structures of many tissues ranging between 0.1 and 1.0 mm [12]. Electrospinning has emerged as one of the methods offering simplicity and versatility in preparing such biomaterials [13]. Electrospun biomaterials facilitate better cell attachment and perfusion due to very high surface area-to-volume ratio and high porosity. Improved cellular response is also suggested because the morphology and architecture of electrospun structure are similar to those of some extracellular matrix (ECM) [14]. In addition, electrospinning may provide an alternative method to produce fibrous materials with improved mechanical properties compared to solid-walled equivalents [15].

Thus, in this study, we used electrospinning to develop scaffolds of fibrous PHA copolymers; P(3HB-*co*-5mol%-3HHx), P(3HB-*co*-7mol%-4HB) and P(3HB-*co*-97mol%-4HB) (Fig. 1), in aim of achieving enhanced biocompatibility, mechanical properties and bioabsorption. We also describe here the characterization and effects of sterilization on the physical properties of the electrospun PHA copolymers. Our study is the first to do a detailed comparison on the bioabsorption rate and the tissue response of electrospun PHA copolymers containing 3HB, 3HHx and 4HB monomers implanted subcutaneously in rat model.

2. Materials and methods

2.1. PHA synthesis

P(3HB-*co*-97mol%-4HB) was biosynthesized by *Delftia acidovorans* (formerly known as *Comamonas acidovorans*) using glucose and 1,4-butanediol as carbon sources, according to the method described in Ref. [16]. P(3HB-*co*-7mol%-4HB) was kindly provided by Dr. Toshihisa Tanaka of RIKEN Institute, Japan. The *in vitro* toxicity of P(3HB-*co*-4HB) derived from *D. acidovorans* has been determined recently [17]. P(3HB) and P(3HB-*co*-5mol%-3HHx) supplied by ICI Biopol and P&G, respectively, were purified before use. Briefly, the purification of the P(3HB) and P(3HB-*co*-5mol%-3HHx) was performed by dissolving the polymers in chloroform followed by precipitation in excess hexane and filtration.

2.2. Fabrication of fibrous implant and electrospinning

Each polymer solution of 1 wt% concentration was prepared by dissolving 100 mg of the polymer in 9900 mg of 1,1,1,3,3,3-hexafluoro-2-propanol (HFIP). Electrospinning was performed using Esprayer ES-2000 (Fuence, Co. Ltd., Japan). The polymer solution was placed in a 1-mL glass syringe with an inner needle diameter of 0.5 mm. The syringe was set vertically at the support of the electrospinning device and the solution was extruded at a constant rate of 40 μl min^{-1}. A positive voltage of 15 kV was applied at a distance of 20 cm between the needle tip and the copper collecting plate. The jet current was in the range of 38.3–38.7 μA and the collecting time was approximately 8 h. For effective collection of the electrospun fibers, a square fiber-collecting area (3 cm × 3 cm) was created on the copper plate by covering the rest of the plate with a non-conductive plastic. A sheet of aluminum foil was used to cover the collection area to ease the recovery of fibrous matrix from the copper plate. Each electrospun PHA scaffold was then cut into two different dimensions: 1 cm × 1 cm and 1 cm × 3 cm, respectively. All scaffolds were sterilized overnight with ethylene oxide (EtO) at 40 °C before implantation in rat.

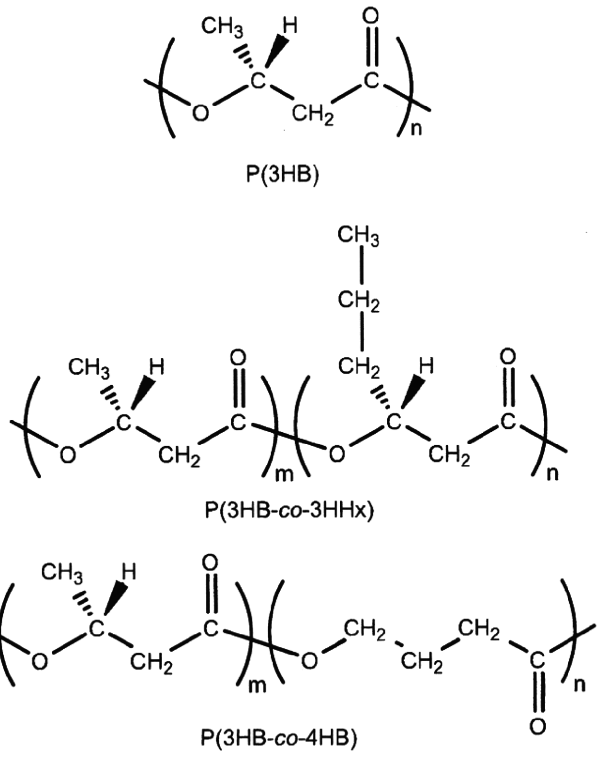

Fig. 1. Chemical structures of PHAs used in this study.

2.3. Subcutaneous implantation in rat and retrieval

Four 12-weeks-old male Wistar rats were used for implanting the PHA scaffolds; two for scaffolds measuring 1 cm × 1 cm while the remaining two for scaffolds measuring 1 cm × 3 cm. The animals were cared for in accordance with the Guiding Principles for the Care and Use of Animals in the Field of Physiological Sciences, approved by the Physiological Society of Japan. All experiment protocols had been reviewed and approved by the Animal Subjects Committee of the National Cardiovascular Center, Osaka, Japan. The rats were first injected with anesthetic before implanting the scaffolds. The 1 cm × 1 cm scaffolds were implanted subcutaneously at one side of the backbone while the 1 cm × 3 cm scaffolds were implanted subcutaneously at the backbone. The grouping of the rats was based on the duration of observation for 4 and 12 weeks. Upon explantation, the scaffolds measuring 1 cm × 1 cm were stored in 2.5% glutaraldehyde solution until further analysis by SEM. The retrieved 1 cm × 3 cm scaffolds were treated with 1.25 wt% trypsin to remove the surrounding tissues. They were then kept in tubes containing phosphate buffered saline (PBS) until further use.

2.4. Scanning electron microscopy

The PHA scaffolds were dehydrated in increasing concentrations of ethanol aqueous solutions containing 50%, 70%, 90%, 95%, 99.5% and 100%. They were then mounted on aluminum stumps and coated with gold in a sputtering device for 3 min at 5 mA. The scaffolds were observed with a scanning electron microscope (JSM-6330F, JEOL, Co. Ltd.) at an acceleration voltage of 5 kV and an emission current of 12 μA.

2.5. Wide-angle X-ray diffraction (WAXD)

Two-dimensional (2D) WAXD patterns of the electrospun PHA scaffolds were acquired using an X-ray diffractometer (RINT UltraX 18, Rigaku Japan) equipped with an imaging plate (BAS-SR 127, Fuji Film Co., Japan). Ni-filtered Cu–K_α radiation ($\lambda = 0.154$ nm) generated at 40 kV and 200 mA was collimated by a pinhole with a diameter of 1.0 mm. The distance from the scaffold to the imaging plate was 5 cm and the exposure time was 6 h. After converting the 2D images to 1D profile by circular-averaging, the crystallinity of the scaffolds was calculated from the ratio of the areas of crystalline reflections to the overall intensity in the range of $12° \leq 2\theta \leq 35°$ of the averaged 1D profile.

2.6. Tensile property

The non-sterilized scaffolds and the scaffolds before and after implantation were cut into 2 mm × 5 mm strips for tensile test. Tensile test on the scaffolds was carried out on a tensile testing machine (SHIMADZU EZTest) at a crosshead speed of 1 mm/min under ambient conditions. The thickness of each scaffold was measured before testing. Tensile properties were calculated from the stress–strain curves as means of two measurements.

2.7. Gel permeation chromatography (GPC) analysis

The molecular weight of the scaffolds was measured with gel permeation chromatography at 40 °C, using a Shimadzu 10A GPC system equipped with a 10A refractive index detector and Shodex K-806M and K-802 columns. Chloroform was used as the eluant at a flow rate of 1.0 ml min^{-1}. The calibration curve was prepared by using polystyrene standards with narrow polydispersity.

2.8. In vitro degradation evaluation

Each of the 1 cm × 3 cm sterilized scaffold was immersed in 10 mL phosphate buffered saline (PBS) at pH 7.4 in sterilized capped containers. These containers were then incubated at 37 °C without agitation. After 4 and 12 weeks, the scaffolds were recovered and characterized by SEM, tensile test, GPC and WAXD.

2.9. Histological observation

The surrounding tissues were excised together with the electrospun PHA scaffolds and fixed with 2.5% glutaraldehyde solution. A small piece of the tissue was then embedded in paraffin before subjecting it to microtome sectioning. Hematoxylin and eosin (HE) were used for staining the tissues. The tissue response to the scaffolds was evaluated from the coloration observed with a phase-contrast microscope.

3. Results and discussion

3.1. Morphological changes of electrospun PHA scaffolds

The retrieved electrospun PHA scaffolds showed various changes in appearances after subcutaneous implantation (Fig. 2). After 4 weeks, both the electrospun P(3HB) and P(3HB-*co*-5mol%-3HHx) remained in their initial form. The electrospun P(3HB-*co*-7mol%-4HB) was fragmented into large pieces while the electrospun P(3HB-*co*-97mol%-4HB) shrunk and became thinner. Even after 12 weeks, the electrospun P(3HB) showed no morphological change. However, significant changes were observed for the other three electrospun PHA copolymers. The degree of degradation increased in the order of P(3HB-*co*-5mol%-3HHx), P(3HB-*co*-7mol%-4HB), and (3HB-*co*-97mol%-4HB). The electrospun P(3HB-*co*-5mol%-3HHx) displayed crevices on its surface while the electrospun P(3HB-*co*-7mol%-4HB) was degraded into small fragments. Only a small piece of the electrospun P(3HB-*co*-97mol%-4HB) scaffold was retrieved, indicating enhanced bioabsorption of this 4HB-rich copolymer.

To have a better understanding on the progress of biodegradation at a fiber scale, SEM was used to observe the morphological changes of the fibers of all the electrospun PHA scaffolds. SEM revealed that all the as-spun scaffolds consist of randomly oriented fibers (Figs. 3 and 4). Further morphological feature is that the fibers fuse together. Namely, the electrospun fibers organize into a three-dimensional network. This is probably because the solvent (HFIP) evaporation was incomplete when the fibers were deposited on the collection plate. The width of the fiber between the junctions was quite uniform. The width decreased in the order of P(3HB) ≈ P(3HB-*co*-5mol%-3HHx) (520 nm) > P(3HB-*co*-97mol%-4HB) (220 nm) > P(3HB-*co*-7mol%-4HB) (190 nm). It has been reported that the width increases proportionally with the molecular weight of the polymer [18]. This is because higher degree of chain entanglement due to high molecular weight is assumed to make it harder for the electrostatic forces to pull, or extend individual chains [19]. Accordingly, the matrices of the electrospun P(3HB) and P(3HB-*co*-5mol%-3HHx) consisted of larger fibers compared to the electrospun P(3HB-*co*-97mol%-4HB) because of their high molecular weight (Table 1).

Interestingly, only the electrospun P(3HB-*co*-7mol%-4HB) formed fibers with irregular shapes with intermittent spindle-like beads on string (Fig. 4A). Possibly the formation of the beaded P(3HB-*co*-7mol%-4HB) fibers is the result of low net charge density. Previous studies have shown that higher net charge density favors the formation of bead-free fibers [20,21]. According to Ref. [20], the net charge density is inversely proportional to the mass of dry polymer (i.e. mass of scaffolds collected from electrospinning), if the other experimental conditions such as jet current, collecting time and polymer concentration are the same. The net charge density decreases in the order of P(3HB-*co*-5mol%-3HHx) (1058 C/l) > P(3HB) (1002 C/l) > P(3HB-*co*-97mol%-4HB) (778 C/l) > P(3HB-*co*-7mol%-4HB) (484 C/l). In this study, the P(3HB-*co*-7mol%-4HB) scaffold had the highest collected mass.

After sterilization, the morphologies observed for the electrospun P(3HB), P(3HB-*co*-5mol%-3HHx) and P(3HB-*co*-7ml%-4HB) remained unchanged (Figs. 3 and 4). The matrix of P(3HB-*co*-97mol%-4HB), however, became less porous

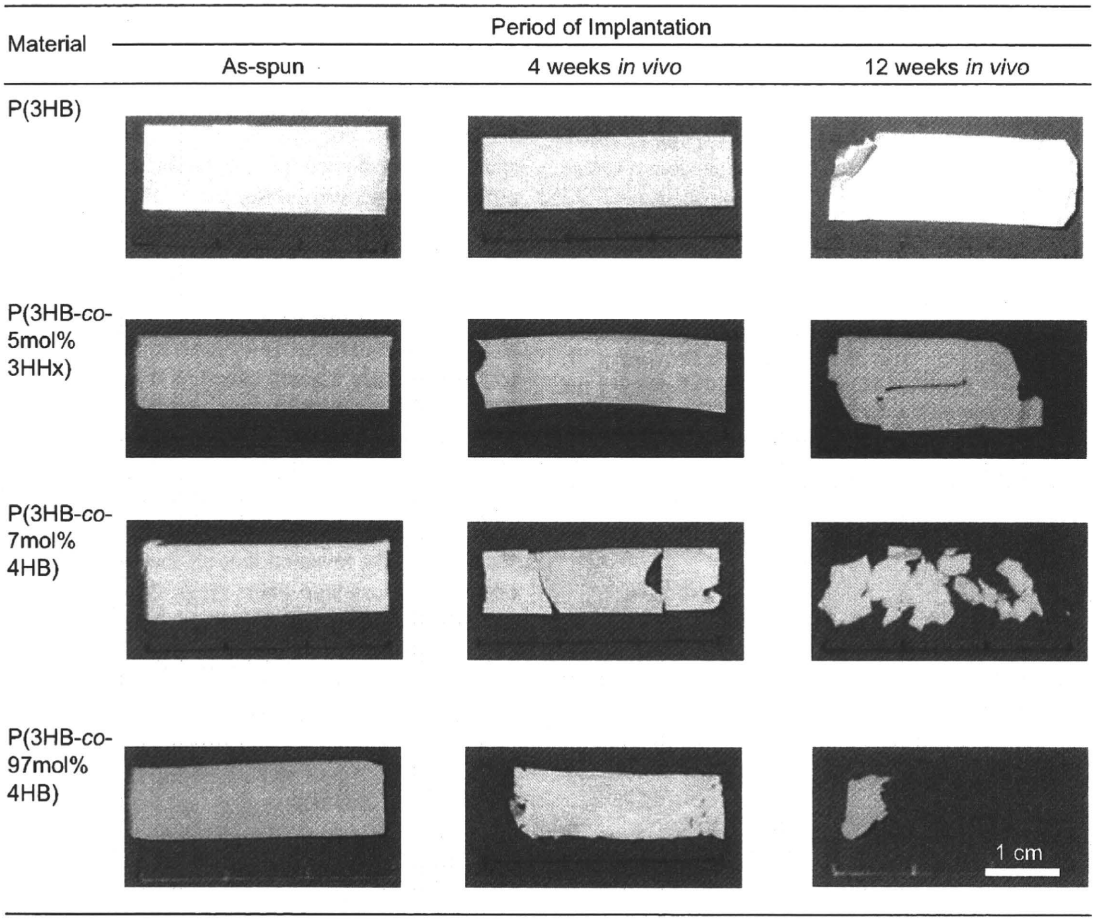

Fig.2. Physical appearance of the electrospun PHA scaffolds before and after 4 and 12 weeks of subcutaneous implantation in rat.

(Fig. 4B2). The temperature (40 °C) of the EtO sterilization is close to the melting temperature of P(3HB-*co*-97mol%-4HB) ($T_m = 47$ °C), and thus led to the fusing of some fibers to each other.

3.1.1. In vivo study

In SEM, only the remaining scaffolds that could be retrieved from rat after the *in vivo* experiments were observed. Nevertheless, such observations provided the information on the morphological changes by implantation. For the P(3HB) and P(3HB-*co*-5mol%-3HHx) scaffolds, no remarkable change in their appearances by implantation during the period investigated here was observed (Fig. 3). This result is in good agreement with the macro-scale observation, as shown in Fig. 2. On the other hand, the fibers of the copolymers with 4HB unit were influenced by the implantation. At 4 weeks of implantation, the fibers of P(3HB-*co*-97mol%-4HB) showed fragmentation (Fig. 4B3). After 12 weeks, surface erosion became more evident as the density of the fibers decreased remarkably due to fragmentation of the fibers to shorter segments. The progression of bioabsorption was also evidenced by the formation of pores on the surface of these fibers as indicated by the arrow in Fig. 4B4. These evidences indicate that the existence of 4HB monomer units enhances the degradability, or the bioabsorption of PHA.

After 4 and 12 weeks, the electrospun P(3HB-*co*-97mol%-4HB) fibers appeared to have swollen (Fig. 4B3 and B4). A slight decrease in the fiber density was also observed for the electrospun P(3HB-*co*-7mol%-4HB) (Fig. 4A4) at week 12. Previous studies have demonstrated that fibers of electrospun poly(D,L-lactic-*co*-glycolic acid), poly(D,L-lactic acid) and poly (butylene succinate) which were highly amorphous showed swelling after immersion in PBS [22–24]. Hence, it is possible that the swelling of the electrospun P(3HB-*co*-97mol%-4HB) fibers occurred due to the penetration of water into their amorphous regions.

3.1.2. In vitro study

SEM showed that there was no evidence of degradation on the surface of all the electrospun PHA scaffolds after 4 weeks of immersion in PBS (Figs. 3 and 4). All samples retrieved at 12 weeks also revealed that their structural integrities were maintained. This is because PHA hardly undergoes hydrolysis at pH value around neutrality. Similar to the observations for the *in vivo* study, the fibers of the electrospun P(3HB-*co*-97mol%-4HB) also demonstrated swelling.

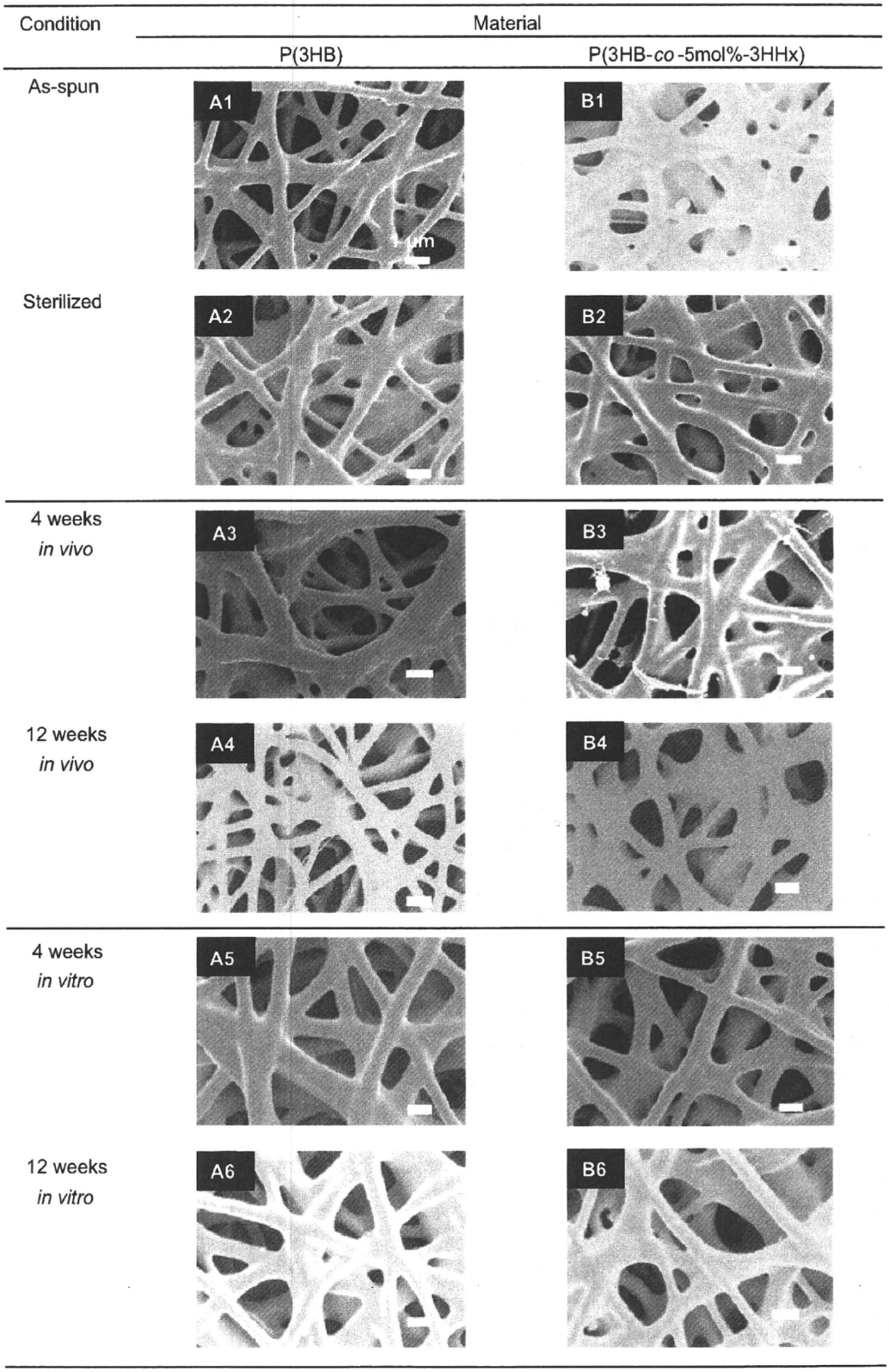

Fig. 3. SEM micrographs of the electrospun P(3HB) and P(3HB-*co*-5 mol%-3HHx) in various conditions.

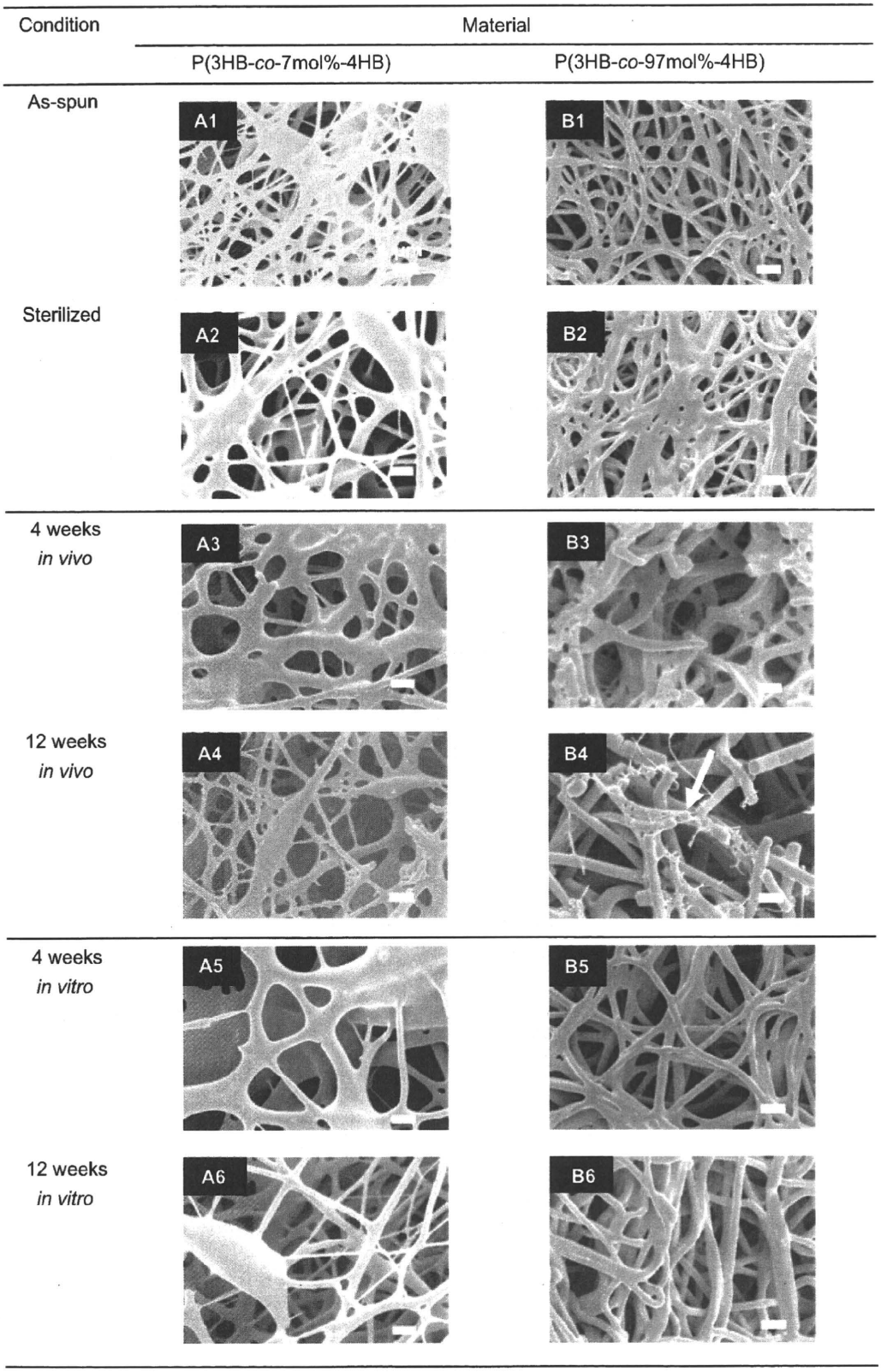

Fig. 4. SEM micrographs of the electrospun P(3HB-*co*-7 mol%-4HB) and P(3HB-*co*-97 mol%-4HB) in various conditions. The arrow shows the pores on the fiber.

Table 1
Molecular weight properties of the electrospun PHA scaffolds

Material	Condition	$M_w \times 10^5$	M_w/M_n
P(3HB)	As-spun	11	3.1
	Sterilized	9.1	3.3
	4 weeks *in vivo*	12	2.6
	4 weeks *in vitro*	11	2.6
	12 weeks *in vivo*	8.5	2.9
	12 weeks *in vitro*	17	3.3
P(3HB-*co*-5mol%-3HHx)	As-spun	13	3.6
	Sterilized	12	3.6
	4 weeks *in vivo*	12	3.1
	4 weeks *in vitro*	11	4.3
	12 weeks *in vivo*	11	3.3
	12 weeks *in vitro*	13	4.3
P(3HB-*co*-7mol%-4HB)	As-spun	7.0	3.0
	Sterilized	6.8	3.0
	4 weeks *in vivo*	6.4	2.6
	4 weeks *in vitro*	6.1	2.6
	12 weeks *in vivo*	3.9	2.7
	12 weeks *in vitro*	5.0	2.6
P(3HB-*co*-97mol%-4HB)	As-spun	1.7	1.5
	Sterilized	1.9	1.8
	4 weeks *in vivo*	1.0	1.6
	4 weeks *in vitro*	2.5	2.0
	12 weeks *in vivo*	1.2	2.0
	12 weeks *in vitro*	2.2	1.8

The *in vivo* and *in vitro* observations using SEM revealed that fibers with smaller diameter were more prone to fragmentation because of increased water contact due to large surface area. Thus, it can be concluded that surface erosion of the electrospun PHA scaffolds depends upon individual fiber dimensions and monomeric content.

3.2. Crystallinity

The WAXD profiles of the as-spun PHA scaffolds are displayed in Fig. 5. The profiles are the ones after subtraction of background. As shown in this figure, the crystalline reflections for the P(3HB) and the 3HB-rich copolymers could be indexed on the basis of P(3HB) α-form structure [25] while the crystalline phase of P(3HB-*co*-97mol%-4HB) fibers adopted the P(4HB) crystal structure [26]. From the 1D profiles, the crystallinity of as-spun, sterilized and scaffolds after *in vivo* and *in vitro* studies is estimated, according to the method described above. As shown in Fig. 6, the crystallinity of the as-spun PHA scaffolds increased in the order of P(3HB-*co*-97mol%-4HB) < P(3HB-*co*-5mol%-3HHx) ≈ P(3HB-*co*-7mol%-4HB) < P(3HB). This tendency is the same as the case of those bulk materials [27]. It has been reported that the crystallinity of P(4HB) homopolymer is much lower than that of P(3HB) homopolymer [28]. The slight lowering of the crystallinities of the 3HB-rich copolymers is due to the exclusion of second monomer unit from the crystalline lattice [29]. It is evident that the degradability of the scaffolds, as shown in Figs. 2 and 3, strongly depends on the crystallinity.

We confirmed that the EtO sterilization did not appear to have any effect on the crystallinities of all the electrospun

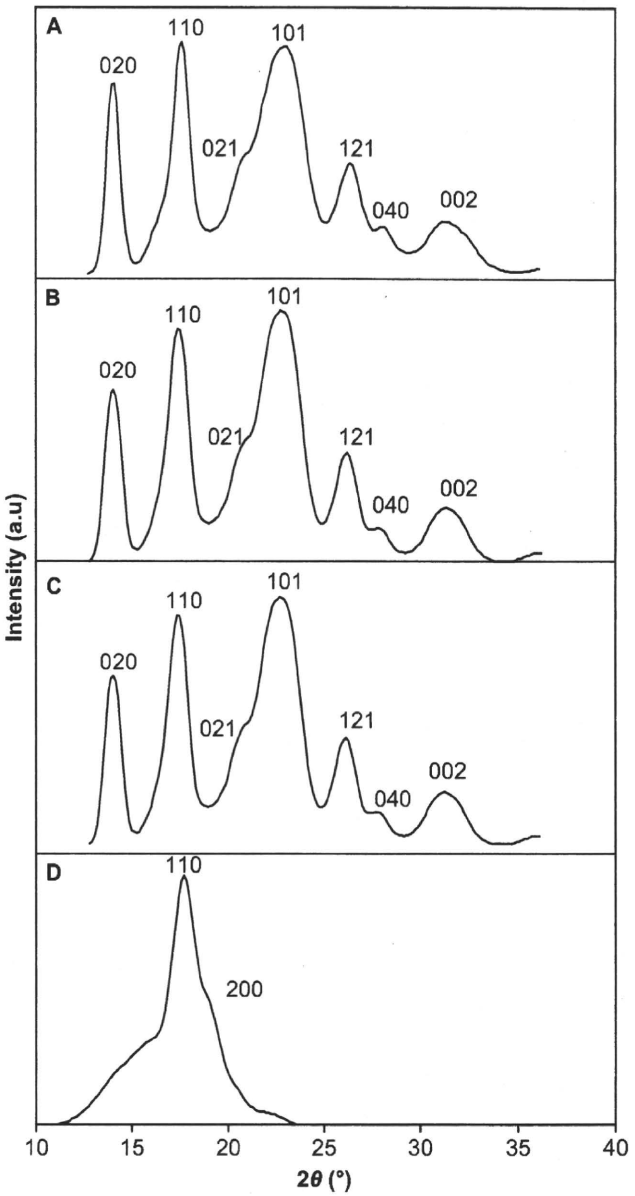

Fig. 5. Integrated 1D profiles from 2D WAXD patterns of as-spun: (A) P(3HB), (B) P(3HB-*co*-5 mol%-3HHx), (C) P(3HB-*co*-7 mol%-4HB) and (D) P(3HB-*co*-97 mol%-4HB).

PHA scaffolds. We described earlier that partial melting might occur during the sterilization of P(3HB-*co*-97mol%-4HB). Even if so, the crystallinity will surely recover after the sterilization. The crystallinities of the scaffolds after the *in vivo* and *in vitro* studies remained unchanged. But, it should be noted that the scaffolds for X-ray measurements are the retrieved or remained ones after *in vivo* and *in vitro* experiments. The crystallinity of the P(3HB-*co*-97mol%-4HB), which shows obvious bioabsorption or degradation in the macro-scale and SEM observations, also little changed even after implantation in rat. This means that the degradation of scaffolds progresses preferentially from the surface of the scaffolds or interface which contacts with the tissues of rat. It is deduced that some substance such as tissue enzymes facilitate the degradation [30].

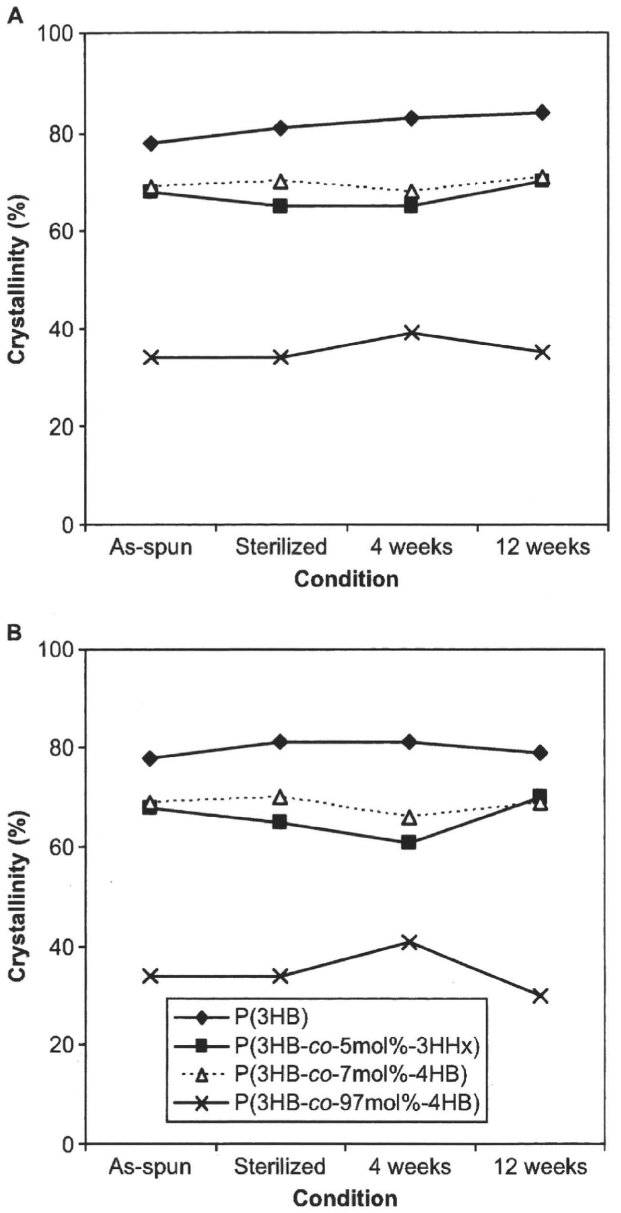

Fig. 6. Crystallinities of the electrospun PHA scaffolds in different conditions: (A) *in vivo* and (B) *in vitro*.

3.3. Molecular weight changes of electrospun PHA scaffolds

Table 1 summarizes the change in M_w and polydispersity index (M_w/M_n) for the as-spun scaffolds and scaffolds following sterilization, 4 and 12 weeks of *in vivo* and *in vitro* studies. After sterilization, all of the electrospun PHA scaffolds showed no significant differences in their molecular weight. Despite the large surface area of the fibers, PHA scaffolds remained intact in the *in vitro* study because they have higher resistance to hydrolysis in non-biological environment where specific enzymes are absent [27,31]. Furthermore, the immersion in PBS (pH 7.4) under sterile conditions up to only 12 weeks is short and the temperature is low for any significant hydrolysis to occur. The subcutaneous implantation, however, seems to cause decrease in the M_w of PHA copolymers with 4HB unit. At 4 weeks, bioabsorption was the most pronounced for the electrospun P(3HB-*co*-97mol%-4HB) with 47% loss M_w, while the M_w of P(3HB-*co*-7mol%-4HB) showed no decrease. Following longer implantation period, the electrospun P(3HB-*co*-7mol%-4HB) lost 43% of M_w. Unexpectedly, the electrospun P(3HB-*co*-97mol%-4HB) recorded only 37% of M_w loss after 12 weeks. It was confirmed that the number of main-chain carbon atom strongly influences the rate of hydrolysis.

3.4. Mechanical properties of electrospun PHA scaffolds

Table 2 summarizes the mechanical properties of electrospun PHA scaffolds obtained. The mechanical properties of all the as-spun scaffolds were comparable to those of human skin, and hence suggest they are mechanically stable in supporting regenerated tissues. The Young's modulus of the as-spun scaffolds increased in the order of P(3HB-*co*-97mol%-4HB) $\ll$ P(3HB-*co*-7mol%-4HB) $<$ P(3HB) $<$ P(3HB-*co*-5mol%-3HHx). Low Young's modulus, that is, high elasticity is a characteristic property in rubber-state amorphous polymers. Accordingly, this

Table 2
Mechanical properties of the PHA scaffolds

Material	Condition	Mechanical properties	
		Tensile strength (MPa)	Young's modulus (MPa)
P(3HB)	As-spun	17	223
	Sterilized	15	234
	4 weeks *in vivo*	12	182
	4 weeks *in vitro*	14	220
	12 weeks *in vivo*	15	152
	12 weeks *in vitro*	13	194
P(3HB-*co*-5mol%-3HHx)	As-spun	15	277
	Sterilized	12	272
	4 weeks *in vivo*	12	268
	4 weeks *in vitro*	13	208
	12 weeks *in vivo*	ND[b]	ND[b]
	12 weeks *in vitro*	15	230
P(3HB-*co*-7mol%-4HB)	As-spun	8	184
	Sterilized	8	139
	4 weeks *in vivo*	ND[b]	ND[b]
	4 weeks *in vitro*	8	163
	12 weeks *in vivo*	ND[b]	ND[b]
	12 weeks *in vitro*	9	110
P(3HB-*co*-97mol%-4HB)	As-spun	13	9
	Sterilized	15	16
	4 weeks *in vivo*	4	12
	4 weeks *in vitro*	11	14
	12 weeks *in vivo*	ND[b]	ND[b]
	12 weeks *in vitro*	14	16
Skin[a]		5–30	15–150

[a] Data obtained from Ref. [13].
[b] Not determined as the retrieved scaffolds from rat had cracks on the surface that prevented tensile test.

indicates that the P(3HB-*co*-97mol%-4HB) fibers are more amorphous than the other scaffolds, and this is consistent with the WAXD results. The distinct mechanical properties of the PHA could find different use as scaffolds for tissue engineering. For example, the 3HB-rich scaffolds which are more rigid could serve as preferential substrates for directional cell migration [32] while the compliant 4HB-rich scaffolds could be used to promote cell motility [33]. The EtO sterilization and the immersion in PBS buffer little affected the mechanical properties of all the scaffolds.

3.5. Histological observation

The histological sections of the electrospun PHA scaffolds at different period of subcutaneous implantation are shown in Fig. 7. Histological observations indicate that all the three electrospun copolymers elicited fairly mild tissue response relative to that of the electrospun P(3HB) throughout the course of study. After 4 weeks of implantation, some parts of the electrospun P(3HB-*co*-97mol%-4HB) bordering the interface were degraded as evidenced by the small fragments broken off from

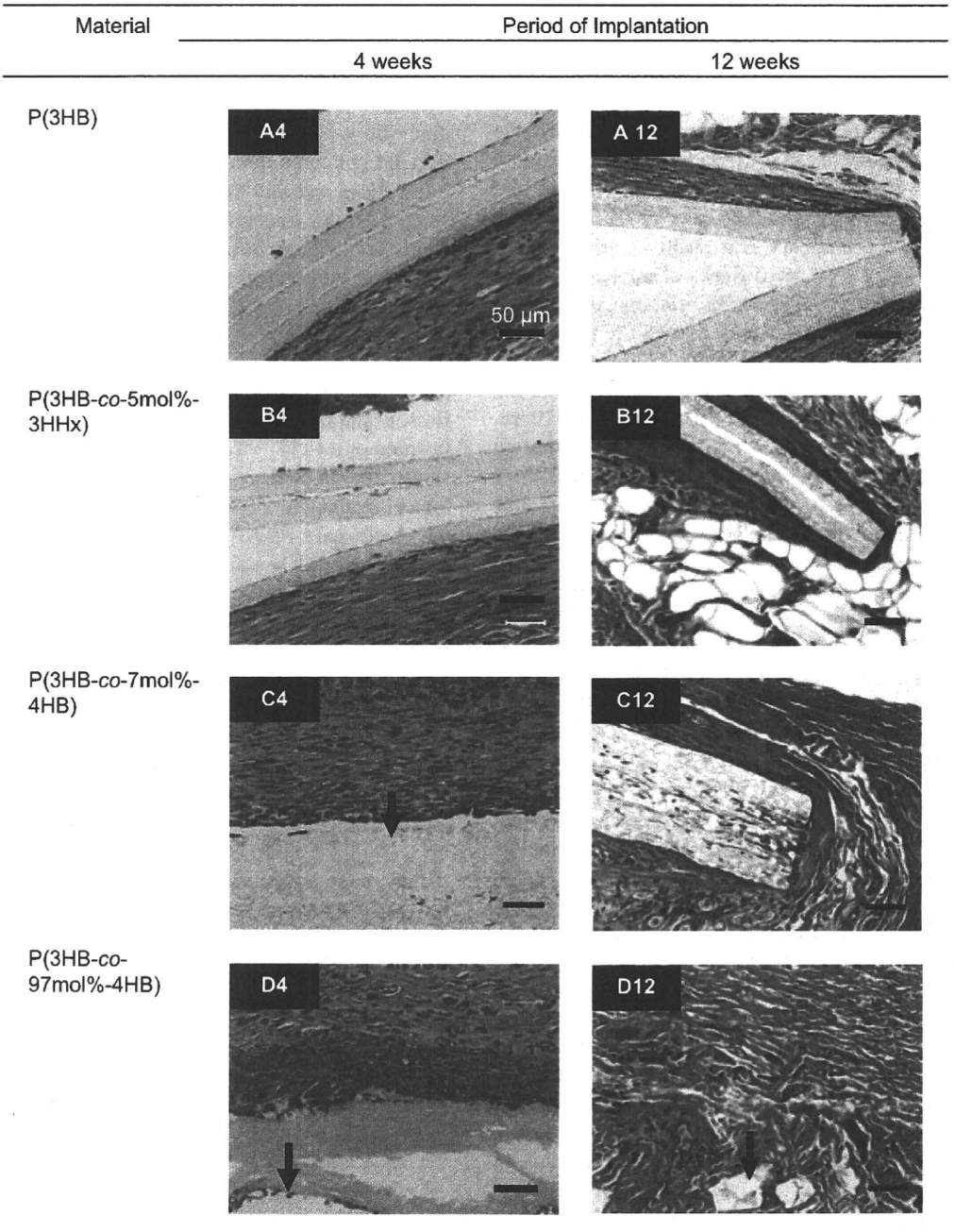

Fig. 7. Histological sections of the electrospun PHA scaffolds at different period of subcutaneous implantation. Arrows indicate the polymer surface.

the main scaffold (Fig. 7D4). More macrophages were found to be present along the interface connected to this copolymer in comparison to the electrospun P(3HB-*co*-7mol%-4HB) and P(3HB-*co*-5mol%-3HHx) (Fig. 7B4 and C4). This phenomenon is desirable during wound healing because the presence of macrophages is necessary for the regeneration of many cell types [34]. The presence of thin connective tissue surrounding the electrospun P(3HB-*co*-97mol%-4HB) was also observed.

The most promising finding was the tissue response after 12 weeks of implantation for the electrospun P(3HB-*co*-97mol%-4HB). No fibrous encapsulation was observed around the degraded copolymer and there was also a substantial drop in the number of inflammatory cells (Fig. 7D12). This observation is similar to a study done on the biocompatibility of P(4HB) implanted subcutaneously in rats by Martin et al. [35], that reported minimal inflammatory responses. In this study, the number of inflammatory cells surrounding the electrospun P(3HB-*co*-7mol%-4HB) and P(3HB-*co*-5mol%-3HHx) did not appear to have lessen. The muscle cells surrounding these two scaffolds appeared compact as a result of inflammatory reaction (Fig. 7B and C). After 12 weeks of implantation, the number of macrophages bordering the electrospun P(3HB) increased. Inflammation was obvious due to the compacted muscle cells surrounding the scaffold. The difference in tissue response to the electrospun P(3HB-*co*-97mol%-4HB) and the electrospun scaffolds with higher molar fraction of 3HB reflected their distinct physical properties. It has been reported that rigid polymer, such as P(3HB), elicit acute inflammatory reaction because it exerts a continuous mechanical stimulus to the surrounding tissues of the implants [36]. Although the tissue response to the electrospun P(3HB-*co*-7mol%-4HB) and electrospun P(3HB-*co*-5mol%-3HHx) was slightly more pronounced than that of the electrospun P(3HB-*co*-97mol%-4HB), the overall local tissue response to all three copolymers was found to be mild. The results have confirmed the biocompatibility of all three types of electrospun PHA copolymers.

3.6. Bioabsorption mechanism

The results from various analyses clearly demonstrated that the bioabsorption rate of the electrospun P(3HB-*co*-97mol%-4HB) was the fastest relative to the other two PHA copolymers. Three possible reasons for this observation are as follows: Firstly, the P(3HB-*co*-97mol%-4HB) with low crystallinity is more susceptible to bioabsorption as water and enzymes penetrate easier into the amorphous regions. Secondly, previous studies have established that macrophages are able to phagocytize PHA *in vitro* [37,38] and free radicals, acidic products or enzymes produced by these cells may also accelerate the degradation [39]. As seen in Fig. 7, the number of inflammatory cells was the most concentrated at the interface of electrospun P(3HB-*co*-97mol%-4HB) suggesting their active part in the bioabsorption process. Thirdly, possibly the enzymatic degradation by lipase also contributed to the rapid bioabsorption of the electrospun P(3HB-*co*-97mol%-4HB). PHA can be enzymatically degraded by PHA depolymerases, but there is no evidence to date that these are present *in vivo* [1]. P(4HB) was found to be also highly susceptible to lipase hydrolysis as opposed to P(3HB) [40]. Besides having good mechanical properties and biocompatibility, it is desirable for a medical implant to show good bioabsorption after its primary function has been fulfilled. The persistence of polymer at a wound healing site may lead to chronic inflammation as shown by the slowly degrading P(3HB) patches that elicited a long-term (greater than 2 years) macrophage response [41]. Hence the fast bioabsorption rates of the electrospun PHA containing 4HB have confirmed their potential in the application for medical implants.

4. Conclusion

In this study, electrospinning proved to be a simple and adaptable fabrication technique in producing constructs with dimensions approaching the native profile of ECM. Sterilization did not cause discoloration and damage to the PHA scaffolds. SEM revealed that both the *in vivo* and *in vitro* surface erosion of the electrospun PHA scaffolds progressed dependently on the individual fiber dimensions and monomeric contents. The mechanical properties demonstrated by all samples were comparable to those of human skin thus suggesting that their structures are able to provide sufficient biomechanical support. The electrospun scaffolds consisting of high 3HB content had higher degree of crystallinity and thus, they showed slower bioabsorption rate. GPC revealed that the *in vitro* degradation of the electrospun PHA scaffolds proceeded at a much slower rate in comparison to the *in vivo* bioabsorption. Histological evaluation showed that subcutaneous implantations of the electrospun PHA scaffolds were well tolerated *in vivo* as the tissue response continued to be very mild throughout the course of the study. Our results revealed that by changing the molar fraction of monomers in the PHA copolymers, it is possible to create tissue-engineering scaffolds that are tailor-made to meet the various needs in regenerating different cell type. The electrospun PHA copolymers proved to be promising biomaterials for scaffolds because of their biodegradability, flexible mechanical properties and excellent biocompatibility.

Acknowledgement

This work was supported by a Grant-in Aid for Scientific Research (B) from the Ministry of Education, Culture, Sports, Science and Technology (MEXT) of Japan (No.19350075) (to T. Iwata) and by a grant for Ecomolecular Science Research II provided by RIKEN Institute.

References

[1] Williams SF, Martin DP. Applications of PHAs in medicine and pharmacy. In: Steinbüchel A, editor. Series of biopolymers in 10 volumes, vol. 4. Wiley/VCY/Verlag; 2002. p. 91–121.

[2] Chen GQ, Wu Q. The application of polyhydroxyalkanoates as tissue engineering materials. Biomaterials 2005;26:6565–78.

[3] FDA clears first of its kind suture made using DNA technology. Available from: FDA News http://www.fda.gov/bbs/topics/NEWS/2007/NEW01560.html; 2007 February 12 [accessed 25.04.07].

[4] Anderson AJ, Dawes EA. Occurrence, metabolic role, and industrial uses of bacterial polyhydroxyalkanoates. Microbial Rev 1990;54:450–72.
[5] Doi Y. Microbial polyesters. New York: VCH; 1990.
[6] Kato M, Bao HJ, Kang CK, Fukui T, Doi Y. Production of a novel copolyester of 3-hydroxybutyric acid and medium-chain-length 3-hydroxyalkanoic acids by *Pseudomonas* sp. 61-3 from sugars. Appl Microbiol Biotechnol 1996;45:363–70.
[7] Hocking PJ, Marchessault RH. Biopolyesters. In: Griffin GJL, editor. Chemistry and technology of biodegradable polymers. London: Chapman & Hall; 1994. p. 48–96.
[8] Nelson T, Kaufman E, Kline E, Sokoloff L. The extraneural distribution of gammahydroxybutyrate. J Neurochem 1981;37:1345–88.
[9] Taylor MS, Daniels AU, Andriano KP, Heller J. Six absorbable polymers: *in vitro* acute toxicity of accumulated degradation products. J Appl Biomat 1994;5:151–7.
[10] Iwata T, Tsunoda K, Aoyagi Y, Kusaka S, Yonezawa N, Doi Y. Mechanical properties of uniaxially cold-drawn films of poly[(*R*)-3-hydroxybutyrate]. Polym Degrad Stab 2003:217–24.
[11] Sudesh K, Abe H, Doi Y. Synthesis, structure and properties of polyhydroxyalkanoates: biological polyesters. Prog Polym Sci 2000;25:1503–55.
[12] Griffith LG. Emerging design principles in biomaterials and scaffolds for tissue engineering. Ann N Y Acad Sci 2000;961:83–95.
[13] Zong X, Bien H, Chung CY, Yin L, Fang D, Hsiao BS, et al. Electrospun fine-textured scaffolds for heart tissue constructs. Biomaterials 2005;26:5330–8.
[14] Li WJ, Laurencin CT, Caterson EJ, Tuan RS, Ko FK. Electrospun nanofibrous structure: a novel scaffold for tissue engineering. J Biomed Res 2002;60:613–21.
[15] Kim J, Reneker DH. Mechanical properties of composites using ultrafine electrospun fibers. Polym Composites 1999;20:124–31.
[16] Lee WH, Azizan MNM, Sudesh K. Effects of culture conditions on the composition of poly(3-hydroxybutyrate-*co*-4-hydroxybutyrate) synthesized by *Comamonas acidovorans*. Polym Degrad Stab 2004;84:129–34.
[17] Siew EL, Rajab NF, Osman A, Sudesh K, Inayat-Hussain SH. *In vitro* biocompatibility evaluation of poly(3-hydroxybutyrate-*co*-4-hydroxybutyrate) copolymer in fibroblast cells. J Biomed Res A 2007;81A:317–25.
[18] Dong H, Nyame V, Macdiarmid Jr AG, Jones WE. Polyaniline/poly(-methyl methacrylate) coaxial fibers: the fabrication and effects of the solution properties on the morphology of electrospun core fibers. J Polym Sci Part B: Polym Phys 2004;42:3934–42.
[19] Lyons J, Li C, Ko F. Melt-electrospinning part I: processing parameters and geometric properties. Polymer 2004;45:7597–603.
[20] Fong H, Chun I, Reneker DH. Beaded nanofibers formed during electrospinning. Polymer 1999;40:4585–92.
[21] Zuo W, Zhu M, Yang W, Yu H, Chen Y, Zhang Y. Experimental study on relationship between jet stability and formation of beaded fibers during electrospinning. Polym Eng Sci 2005;45:704–9.
[22] Zong X, Ran S, Kim KS, Fang D, Hsiao BS, Chu B. Structure and morphology changes during *in vitro* degradation of electrospun poly(glycolide-*co*-lactide nanofiber membrane. Biomacromolecules 2003;4:416–23.
[23] Li WJ, Cooper Jr JA, Mauck RL, Tuan RS. Fabrication and characterization of six electrospun poly(α-hydroxyester)-based fibrous scaffolds for tissue engineering applications. Acta Biomaterialia 2006;2:377–85.
[24] Jeong EH, Im SS, Youk JH. Electrospinning and structural characterization of ultrafine poly(butylenes succinate) fibers. Polymer 2005;4:9538–43.
[25] Yokouchi M, Chatani Y, Tadokoro H, Teranishi K, Tani H. Structural studies of polyesters: 5. Molecular and crystal structures of optically active and racemic poly (β-hydroxybutyrate). Polymer 1973;14:267–72.
[26] Su F, Iwata T, Tanaka F, Doi Y. Crystal structure and enzymatic degradation of poly(4-hydroxybutyrate). Macromolecules 2003;36:6401–9.
[27] Doi Y, Kanesawa Y, Kawaguchi Y, Kunioka M. Biodegradation of microbial polyesters in the marine environment. Polym Degrad Stab 1992;32:173–7.
[28] Mitomo H, Hsieh WC, Nishiwaki K, Kasuya K, Doi Y. Poly(3-hydroxybutryate-co-4-hydroxybutyrate) produced by *Comamonas acidovorans*. Polymer 2001;42:3455–61.
[29] Di Lorenzo ML, Raimo M, Cascone E, Martuscelli E. Poly(3-hydroxybutyrate)-based copolymers and blends: influence of a second component on crystallization and thermal behavior. J Macromol Sci Phys 2001;40:639–67.
[30] Gogolewski S. Resorbable polymers for internal fixation. Clin Mater 1992;10:13–20.
[31] Marois Y, Zhang Z, Vert M, Deng X, Lenz R, Guidoin R. Mechanism and rate of degradation of polyhydroxyoctanoate films in aqueous media: a long term *in vitro* study. J Biomed Mater Res 2000;49:216–24.
[32] Lo CM, Wang HB, Dembo M, Wang YL. Cell movement is guided by the rigidity of the substrate. Biophys J 2000;79:144–52.
[33] Pelham RJ, Wang YL. Cell locomotion and focal adhesions are regulated by substrate flexibility. Proc Natl Acad Sci U S A 1997;94:13661–5.
[34] Rappolee DA, Mark D, Banda MJ, Werb Z. Wound macrophages express TGF-alpha and other growth factors *in vivo*: analysis by mRNA phenotyping. Science 1988;241:708.
[35] Martin DP, Skraly FA, Williams SF. Polyhydroxyalkanoate compositions having controlled degradation rats. PCT Patent Application No. WO 99/32536; 1999.
[36] Qu XH, Wu Q, Zhang KY, Chen GQ. *In vivo* studies of poly(3-hydroxybutyrate-*co*-3-hydroxyhexanoate) based polymers: biodegradation and tissue reactions. Biomaterials 2006;27:3540–8.
[37] Ali SAM, Doherty PJ, Williams DF. Molecular biointeractions of biomedial polymers with extracellular exudates and inflammatory cells and their effects on the biocompatibility *in vivo*. Biomaterials 1994;15:779–85.
[38] Saad B, Neuenschwander P, Uhlschmid GK, Suter UW. New versatile, elastomeric, degradable polymeric materials for medicine. Intern J Biol Macromol 1999;25:293–301.
[39] Tracy MA, Ward KL, Firouzabadian L, Wang Y, Dong N, Qian R, et al. Factors affecting the degradation rate of poly(lactide-*co*-glycolide) microspheres *in vivo* and *in vitro*. Biomaterials 1999;20:1057–62.
[40] Mukai K, Doi Y, Sema Y, Tomita K. Substrate specificities in hydrolysis of polyhydroxyalkanoates by microbial esterases. Biotechnol Lett 1993;15:601–4.
[41] Malm T, Bowald S, Bylock A, Busch C, Saldeen T. Enlargement of the right ventricular outflow tract and the pulmonary artery with a new biodegradable patch in transanular position. Eur Surg Res 1994;26:298–308.

Peptide Science 2007: S. Aimoto and S. Ono (Eds.)
The Japanese Peptide Society (2008)

Fundamental Studies on Genetically Engineered Elastin Model Peptides for Biomaterials

Sachiro Kakinoki[1], Alyssa Panitch[2], David A. Tirrell[3], and Tetsuji Yamaoka[1]

[1]Department of Biomedical Engineering, National Cardiovascular Center Research Institute, 5-7-1 Fujishirodai, Suita, Osaka 565-8565, Japan, [2]Weldon School of Biomedical Engineering, Purdue University, IN 47907, USA, and [3]Department of Chemical Engineering, California Institute of Technology, CA 91125, USA
e-mail: yamtet@ri.ncvc.go.jp

Elastin model peptide ((Val-Pro-Gly-Ile-Gly)$_{40}$; VPGIG$_{40}$) was designed and biosynthesized as injectable scaffold for cell transplantation therapies. In this report, the thermoresponsiveness and the potential as the base materials for injectable scaffold of VPGIG$_{40}$ expressed using genetic-engineering technique were explored.

Keywords: biomaterials, elastin model peptide, genetic engineering, injectable scaffold, thermoresponsiveness

Introduction

Recently, cell transplantation therapies are much attended with progress of regenerative medicine and stem-cell research. It is known that substantial effects can not be obtained only by injecting the cell suspensions and then feasible scaffolds are necessary for the cell transplantation therapies. Therefore, various biodegradable polymeric materials have been investigated as scaffolds actively. However, these scaffolds are not suitable for the cell transplantation therapy, because these bulk-type scaffolds require invasive surgery, and the cells inside the scaffold often necrotize. In order to solve these problems, photo-crosslinkable and thermoresponsible hydrogels have been investigated as injectable scaffolds. However, these non-biodegradable materials are not approved for the clinical use yet.

Elastin, the major component of elastic fibers in basement membrane, provides the resilience or restorative force to tissues. Noteworthy, soluble elastin-related polypeptides, such as tropoelastin, α-elastin and synthetic elastin model peptides, indicate the characteristics of temperature-depending phase transition. Therefore, we are interested in the potential of elastin model peptides as injectable scaffolds. In this report, we try to biosynthesize and characterize an elastin model peptide ((Val-Pro-Gly-Ile-Gly)$_{40}$; VPGIG$_{40}$) and develop the gel matrices consisting of VPGIG$_{40}$ to apply as injectable scaffold.

Results and Discussion

The elastin model peptides with repetitive sequence, VPGIG$_{40}$, were biosynthesized using *E. coli* [BL21(DE3)pLysS] which was transformed with an

expression-vector encoding VPGIG sequence [pET-28ap ($VPGIG_{40}$)] [1]. The insert region in pET-28ap ($VPGIG_{40}$) was confirmed by direct PCR of *E. coli* using primers which were flanking sequence of the insert region. By agarose electrophoresis, a band was observed at approximately 650 bp corresponding to the DNA length for the insert region of $VPGIG_{40}$. Protein expression was induced with the addition of β-isopropyl thiogalactoside (IPTG) and was allowed to continue for 24 hours. Protein purification was performed using the thermoresponsible property of $VPGIG_{40}$, namely, $VPGIG_{40}$ was purified with temperature control over/below the transition temperature. By SDS-PAGE, it is confirmed that crude $VPGIG_{40}$ was gradually purified by repeating this method and a clear band was indicated at approximately 18 kDa (Fig. 1). The purified $VPGIG_{40}$ was also confirmed by MALDI-TOF/MS analysis.

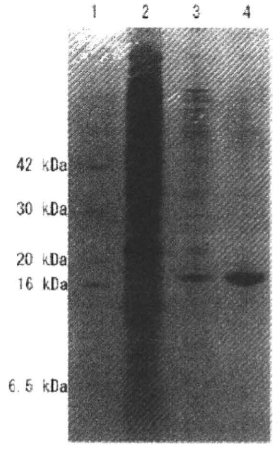

Fig. 1. SDS-PAGE (12%) for elastin model peptide $VPGIG_{40}$ at each purification step. (lane 1; marker, lane 2; bacterial lysate, lane 3; peptide purified once, lane 4; peptide purified twice)

Furthermore, the cloud points of purified $VPGIG_{40}$ were 28.2, 23.6 and 21.9 ℃ at 0.02, 0.05 and 0.1 w/v%, respectively. The mechanism for the temperature-depending phase transition of $VPGIG_{40}$ in solution has been suggested that the peptides are aggregated by hydrophobic interaction with conformational change from random-coil to β-spiral [2, 3].

The results suggest that genetically engineered $VPGIG_{40}$ has high potential as injectable scaffold for cell transplantation.

Acknowledgement

We are grateful to Prof. Shigeru Kunugi at Kyoto Institute of Technology.

References

1. Panitch, A., Yamaoka, T., Fournier, M. J., Mason, T. L., Tirrell, D. A. (1999) *Macromolecules*, **32**, 1701-1703.
2. Tamura, T., Yamaoka, T., Kunugi, S., Panitch, A., T., Tirrell, D. A. (2000) *Biomacromolecules*, **1**, 552-555.
3. Yamaoka, T., Tamura, T., Seto, Y., Tada, T., Kunugi, S., Tirrell, D. A. (2003) *Biomacromolecules*, **4**, 1680-1685.

Acta Biomaterialia 6 (2010) 1925–1930

Contents lists available at ScienceDirect

Acta Biomaterialia

journal homepage: www.elsevier.com/locate/actabiomat

Stable modification of poly(lactic acid) surface with neurite outgrowth-promoting peptides via hydrophobic collagen-like sequence

Sachiro Kakinoki, Tetsuji Yamaoka *

Department of Biomedical Engineering, National Cardiovascular Center Research Institute, 5-7-1 Fujishirodai, Suita, Osaka 565-8565, Japan
JST, CREST, 5 Sanbancho, Chiyoda-ku, Tokyo 102-0075, Japan

ARTICLE INFO

Article history:
Received 30 July 2009
Received in revised form 11 November 2009
Accepted 1 December 2009
Available online 5 December 2009

Keywords:
Surface modification
PLA scaffold
Peptide adsorption
Hydrophobic interaction
Neurite outgrowth-promoting peptide

ABSTRACT

Surface modification of poly(DL-lactic acid) (PLA) scaffolds has been performed using a biofunctional small peptide composed of collagen-like repetitive sequence and laminin-derived sequence (AG73-G_3-$(PPG)_5$) via hydrophobic interaction. The results of surface analysis suggest that AG73-G_3-$(PPG)_5$ can be stably adsorbed onto PLA films via hydrophobic interaction at the $(PPG)_5$ region, and form an extracellular matrix-like layer composed of both structural and biosignalling sequences. In addition, neurite outgrowth of PC12 cells was observed on the AG73-G_3-$(PPG)_5$-adsorbed PLA film. These results indicate that AG73-G_3-$(PPG)_5$ very effectively enhances neurite outgrowth activity on PLA films. The hydrophobic adsorption of collagen-like peptide bound to biosignalling molecules may be widely applied as a surface modifier of PLA films for tissue engineering.

1. Introduction

Tissue engineering has been proposed as an approach to replace damaged, injured or missing tissue with biologically compatible substrate combining cells or biosignalling molecules and scaffolds [1,2]. Scaffolds assume the role of a temporary extracellular matrix (ECM) where biodegradability and biocompatibility are essential for tissue regeneration. Furthermore, biodegradable scaffolds should be designed not to obstruct tissue regeneration via cell-induced natural healing. The cellular responses to the scaffold surfaces determine whether tissue regeneration will be promoted or obstructed. Therefore, it is very important to control the biological property of the scaffold surfaces [3].

Poly(lactic acid) (PLA) is widely used for biodegradable scaffolds as it possesses a number of suitable characteristics for this role. PLA can be hydrolytically degraded into lactic acid; this degradation requires only water, and the final product can immediately be metabolized in vivo [4]. Moreover, PLA material exhibits excellent shaping and molding properties because of its mechanical versatility. However, insufficient interaction between PLA materials and cells leading to in vivo foreign-body reactions is a major problem because the required biological activities are not inherent in PLA. PLA lacks functional groups and so cannot be easily modified with bioactive molecules. Therefore, many investigators have attempted to impart functional groups to PLA in order to enhance its biological activity by using copolymerization or chemical grafting with other polymers [5], plasma treatment [6], chemical modification [7] and physical adsorption. In previous studies, we reported on the preparation of poly(lactic-co-malic acid)-conjugated Arg-Gly-Asp (RGD) tripeptide [8] and gelatin-immobilized PLA scaffold [9] in order to improve the cell attachment. However, because these techniques are prone to adverse chemical reactions, it is necessary to develop techniques that are simpler and offer better biocompatibility. Physical adsorption, which is driven by electrostatic, hydrophobic and specific interactions, has been noted as a simpler surface modification technique of PLA scaffolds [10–12].

In the current work, neurite outgrowth-promoting peptides, consisting of laminin-derived sequence and collagen-like sequence, were designed as surface modifiers of PLA films via hydrophobic adsorption. PLA is preferred as a base material for a nerve regeneration conduit because of its excellent shaping and molding properties [13]. However, PLA does not inherently cater to any nerve regeneration activity. If biologically modified PLA-based artificial nerve can promote nerve regeneration, it might be possible to avoid donor site defects in autologous nerve transplantation. It was reported that laminin-derived sequence AG73 supports neurite outgrowth [14], and therefore was selected as a nerve-regenerating peptide.

On the other hand, it is well known that collagen is a predominant component of ECM [15,16]. The major part of collagen

* Corresponding author. Address: Department of Biomedical Engineering, National Cardiovascular Center Research Institute, 5-7-1 Fujishirodai, Suita, Osaka 565-8565, Japan. Tel.: +81 6 6833 5012x2637; fax: +81 6 6835 5476.
E-mail address: yamtet@ri.ncvc.go.jp (T. Yamaoka).

1742-7061/$ - see front matter © 2009 Acta Materialia Inc. Published by Elsevier Ltd. All rights reserved.
doi:10.1016/j.actbio.2009.12.001

consists of Xaa-Yaa-Gly repetitive sequences, where Xaa and Yaa positions are often occupied by Pro and 4(R)-hydroxyproline (Hyp), respectively, and forms the hydrophobic polyproline-II (PP-II) structure [17–20]. The collagen triple-helix structure is composed of three PP-II chains, and collagen-like peptides (CLPs) such as $(Pro\text{-}Pro\text{-}Gly)_n$ are also able to form a triple-helix structure [21–23]; therefore, CLP is expected to be adsorbed by PLA films via hydrophobic interaction. Animal-derived collagen has also been intensively investigated as a conduit for nerve regeneration because of its high bioactivity [24]. However, animal-derived collagens possess high antigenicity in vivo because of the unnecessary biosignal sequences and enzymatically digested fragments [25]. CLP, which is the repetitive sequence at a structural region of collagen without any enzyme-digestible sequence, is anticipated to be of low immunogenicity.

Here, we are reporting on a neurite outgrowth-promoting peptide composed of AG73 and CLP (AG73-G_3-$(PPG)_5$) as a surface modifier of PLA films for tissue engineering. Conformation of AG73-G_3-$(PPG)_5$ was studied by circular dichroism (CD) spectroscopy. The surface characteristics of AG73-G_3-$(PPG)_5$-adsorbed PLA film were investigated by water contact angle measurement and X-ray photoelectron spectroscopy (XPS). PC12 cells were primed with nerve growth factor (NGF) and cultured on the AG73-G_3-$(PPG)_5$-adsorbed PLA films, and the neurite outgrowth activity was then quantified.

2. Materials and methods

2.1. Materials

$(PPG)_{10}$, AG73 (RKRLQVQLSIRT) and AG73-G_3-$(PPG)_5$ were commercially synthesized by SCRUM, Inc. (Tokyo, Japan). PLA (Mw 130,000) was obtained from Mitsui Chemicals, Inc. (Tokyo, Japan). Progesterone, sodium selenite (N_2SeO_3) and transferrin were purchased from Nacalai Tesque, Inc. (Kyoto, Japan). NGF and horse serum (HS) were obtained from Sigma–Aldrich, Inc. (St. Louis, MO, USA). Insulin, advanced DMEM/F12 and penicillin–streptomycin were purchased from Invitrogen Corporation (Carlsbad, CA, USA). Fetal bovine serum (FBS) was obtained from MP Biomedicals, Inc. (Solon, OH, USA).

2.2. Methods

2.2.1. Circular dichroism

CD spectra were measured by a J-720 spectropolarimeter (Jasco Co., Tokyo, Japan) with a standard analysis program. The temperature was controlled using a recirculating waterbath and spectra was recorded with a 0.1 cm path length cell, using a scanning speed 10 nm min^{-1}, with a 1.0 nm spectral bandwidth, over the wavelength range from 190 to 250 nm. Peptides were dissolved with water at 0.25 mM. Data are represented in molar elipticities ($[\theta]$ deg cm^2 $dmol^{-1}$).

2.2.2. Peptide adsorption on PLA films

PLA films (diameter $\varphi = 6.0$ mm; $t = 0.5$ mm) were prepared with a hot shrinking machine at 180 °C and sterilized by UV irradiation. Three peptides, $(PPG)_{10}$, AG73, and AG73-G_3-$(PPG)_5$, were dissolved in sterilized water at 10 μM, and then 1 ml of each peptide solution was poured onto a PLA film in a 24-well cell culture plate. Peptide solutions were dried for 24 h. In order to get rid of any excessively adsorbed peptide, the PLA films were washed with 1 ml of sterilized H_2O or 1.0 M NaCl aqueous solution twice for 30 min, and then the films were washed with 1 ml of sterilized H_2O again and dried in vacuo.

2.2.3. Water contact angle

The contact angle with distilled water was measured by using a contact-angle meter (CA-X; Kyowa Interface Science Co., Ltd., Saitama, Japan). Images of the water spreading on the sample were recorded by a camera and then analyzed. Three samples were measured for each group.

2.2.4. X-ray photoelectron spectroscopy

The surface composition of peptide-adsorbed PLA films was determined using an ESCA-3400 (Shimadzu Co., Kyoto, Japan). The X-ray source was a monochromatic Mg K_α X-ray from a rotating anode. Survey scans were measured from 0 to 1200 eV. Peak positions and areas were analyzed and ratios for C1s, N1s and O1s were calculated by using software provided by the manufacturer.

2.3. Cell culture

Rat adrenal pheochromocytoma PC12 cells (RIKEN BioResource Center, Ibaraki, Japan) were maintained in DMEM supplemented with 100 U ml^{-1} penicillin, 100 μg ml^{-1} streptomycin, 10% FBS and 7.5% HS. PC12 cells were cultured in poly-D-Lys coated cell-culture dishes (BD, NJ, USA) and maintained at 37 °C in an atmosphere of 5% CO_2 and 95% air.

2.4. Neurite outgrowth assay

The neurite outgrowth assay was performed by using PC12 cells as the model of neural stem cells [26]. PC12 cells were primed with 100 ng ml^{-1} NGF for 24 h on polystyrene cell-culture dishes. The cells were then collected by agitation and placed in the culture medium for 30 min at 37 °C in an atmosphere of 5% CO_2 and 95% air. The cells were washed and resuspended with advanced DMEM/F12 containing 5 μg ml^{-1} insulin, 100 ng ml^{-1} NGF, 20 nM progesterone, 30 nM Na_2SeO_3 and 100 mg ml^{-1} transferrin. The cells were then seeded on peptide-adsorbed PLA films at a seeding density of 2.0×10^4 cells $film^{-1}$ in 24-well cell culture plates, and incubated at 37 °C for 24 h. PC12 cells on peptide-adsorbed PLA films were fixed with 10% formalin and stained by 4% crystal violet/methanol solution, and then the number of PC cells with or without neurites was determined in order to evaluate the neurite outgrowth activity as described elsewhere [27,28]. The lengths of neurites were measured using software (Image J; National Institute of Mental Health, MD, USA) [29]. Cells with neurites longer than 50 μm and those with neurites shorter than 50 μm were counted separately.

3. Results and discussion

3.1. Secondary structure of peptides

The CD spectra of $(PPG)_{10}$, AG73 and AG73-G_3-$(PPG)_5$ are shown in Fig. 1. The CD spectrum of $(PPG)_{10}$ in water at 37 °C exhibited a strong negative band at 209 nm and a positive band at 229 nm, which are known as typical patterns of collagen triple-helix and PP-II structure [20,30]. Although the CD spectrum of PP-II is similar to that of collagen triple-helix, the transition temperature of $(PPG)_{10}$ is reported to be about 28 °C in water [31]. Therefore, this CD spectrum indicates that $(PPG)_{10}$ forms the PP-II structure. The CD spectrum of AG73 showed a strong negative band at 199 nm, assigned as a random-coil structure. In the case of AG73-G_3-$(PPG)_5$, the CD spectrum indicated an intermediate pattern between $(PPG)_{10}$ and AG73. This means that a negative band was blue-shifted and a positive band at 229 nm was decreased in comparison with $(PPG)_{10}$. In addition, all CD spectra have an isosbestic